Bioactive Materials 34 (2024) 37–50

Contents lists available at ScienceDirect

Bioactive Materials

journal homepage: www.keaipublishing.com/en/journals/bioactive-materials

Lysosomal destabilization: A missing link between pathological calcification and osteoarthritis

Tao Ye [a,1], Chenyu Wang [a,1], Jianfei Yan [b,1], Zixuan Qin [a], Wenpin Qin [b], Yuxuan Ma [a], Qianqian Wan [a], Weicheng Lu [b], Mian Zhang [a], Franklin R. Tay [c,**], Kai Jiao [b,***], Lina Niu [a,*]

[a] State Key Laboratory of Oral & Maxillofacial Reconstruction and Regeneration & National Clinical Research Center for Oral Diseases & Shaanxi Key Laboratory of Stomatology, Department of Prosthodontics, School of Stomatology, The Fourth Military Medical University, Xi'an, Shaanxi, 710032, PR China
[b] Department of Stomatology, Tangdu Hospital, State Key Laboratory of Oral & Maxillofacial Reconstruction and Regeneration & National Clinical Research Center for Oral Diseases & Shaanxi Key Laboratory of Stomatology, School of Stomatology, The Fourth Military Medical University, Xi'an, Shaanxi, 710032, PR China
[c] The Dental College of Georgia, Augusta University, Augusta, GA, 30912, USA

ARTICLE INFO

Keywords:
Osteoarthritis
Hydroxyapatite
Lysosomal destabilization
Chondrocyte pyroptosis
Pathological calcification

ABSTRACT

Calcification of cartilage by hydroxyapatite is a hallmark of osteoarthritis and its deposition strongly correlates with the severity of osteoarthritis. However, no effective strategies are available to date on the prevention of hydroxyapatite deposition within the osteoarthritic cartilage and its role in the pathogenesis of this degenerative condition is still controversial. Therefore, the present work aims at uncovering the pathogenic mechanism of intra-cartilaginous hydroxyapatite in osteoarthritis and developing feasible strategies to counter its detrimental effects. With the use of *in vitro* and *in vivo* models of osteoarthritis, hydroxyapatite crystallites deposited in the cartilage are found to be phagocytized by resident chondrocytes and processed by the lysosomes of those cells. This results in lysosomal membrane permeabilization (LMP) and release of cathepsin B (CTSB) into the cytosol. The cytosolic CTSB, in turn, activates NOD-like receptor protein-3 (NLRP3) inflammasomes and subsequently instigates chondrocyte pyroptosis. Inhibition of LMP and CTSB *in vivo* are effective in managing the progression of osteoarthritis. The present work provides a conceptual therapeutic solution for the prevention of osteoarthritis via alleviation of lysosomal destabilization.

1. Introduction

Osteoarthritis is the most common form of arthritis. This degenerative condition worsens over time as the cartilage is progressively worn away. The development of osteoarthritis has been affiliated with inflammation [1–4]. Osteoarthritis results in physical disability and affects over 500 million people worldwide, creating colossal economic and public health burdens [5]. The clinical management of osteoarthritis is challenging. Contemporary mainstream therapies that focus on pain and inflammation reduction are not adept at halting or retarding disease progression [6–9]. This is probably attributed to incomplete understanding of origin of the associated inflammatory responses [1,2,6]. Cartilage calcification by hydroxyapatite has been recognized as a hallmark of osteoarthritis and presumably initiate osteoarthritis. It strongly correlates with the severity of osteoarthritis, but no strategies are available to prevent crystal deposition and permit mineral dissolution in osteoarthritic cartilage so far [10–12]. The hydroxyapatite crystallites within osteoarthritic cartilage have been associated with inflammation in osteoarthritis [11–14]. However, the exact mechanism in which hydroxyapatite initiates inflammation is contentious [11].

The pro-inflammatory cytokine interleukin-1 beta (IL-1β) is the major mediator of cartilage degeneration in osteoarthritis. This cytokine

Peer review under responsibility of KeAi Communications Co., Ltd.
* Corresponding author. The Fourth Military Medical University, Xi'an, Shaanxi, PR China.
** Corresponding author. Augusta University, Augusta, GA, USA.
*** Corresponding author. The Fourth Military Medical University, Xi'an, Shaanxi, PR China.
E-mail addresses: yetaofmmu@foxmail.com (T. Ye), 761029049@qq.com (C. Wang), 2415066075@qq.com (J. Yan), 2301271704@qq.com (Z. Qin), qinwenpin1112@163.com (W. Qin), mayuxuan95@163.com (Y. Ma), 867684246@qq.com (Q. Wan), 291107976@qq.com (W. Lu), zhangmian1986@aliyun.com (M. Zhang), ftay@augusta.edu (F.R. Tay), kjiao1@163.com (K. Jiao), niulina831013@126.com (L. Niu).
[1] These authors contributed equally to the manuscript.

https://doi.org/10.1016/j.bioactmat.2023.12.001
Received 22 August 2023; Received in revised form 10 November 2023; Accepted 1 December 2023

causes extracellular matrix degradation of the osteoarthritic cartilage [1,15]. However, IL-1β inhibition is ineffective in the management of osteoarthritis in human clinical trials [16,17]. This dilemma may be attributed to the intervention of the osteoarthritic inflammatory cascade caused by upstream signaling molecules of IL-1β. Inflammasomes are cytoplasmic multi-protein complexes comprising a sensor protein and inflammatory caspases. The NOD-like receptor protein-3 (NLRP3) inflammasome is a classical regulator of IL-1β production and is responsible for triggering inflammatory responses in osteoarthritis [18–20]. In crystal deposition diseases such as gout or atherosclerosis, NLRP3 inflammasomes are activated by different types of crystallites; in some instances, inflammation is amplified by pyroptosis of the resident cells [18,21–23]. However, it is not known whether extracellular hydroxyapatite crystallites produced during the progression of osteoarthritis are involved in the activation of intracellular NLRP3 inflammasomes and the induction of chondrocyte pyroptosis.

Lysosomes are hydrolases-loaded intracellular organelles involved in the digestion of external agents [24]. Extracellular crystallites phagocytized by lysosomes resulted in lysosomal destabilization, a phenomenon that is characterized by lysosomal membrane permeabilization (LMP) [21,25]. The latter causes the release of hydrolases such as cathepsin B (CTSB), which is a potent activator of NLRP3

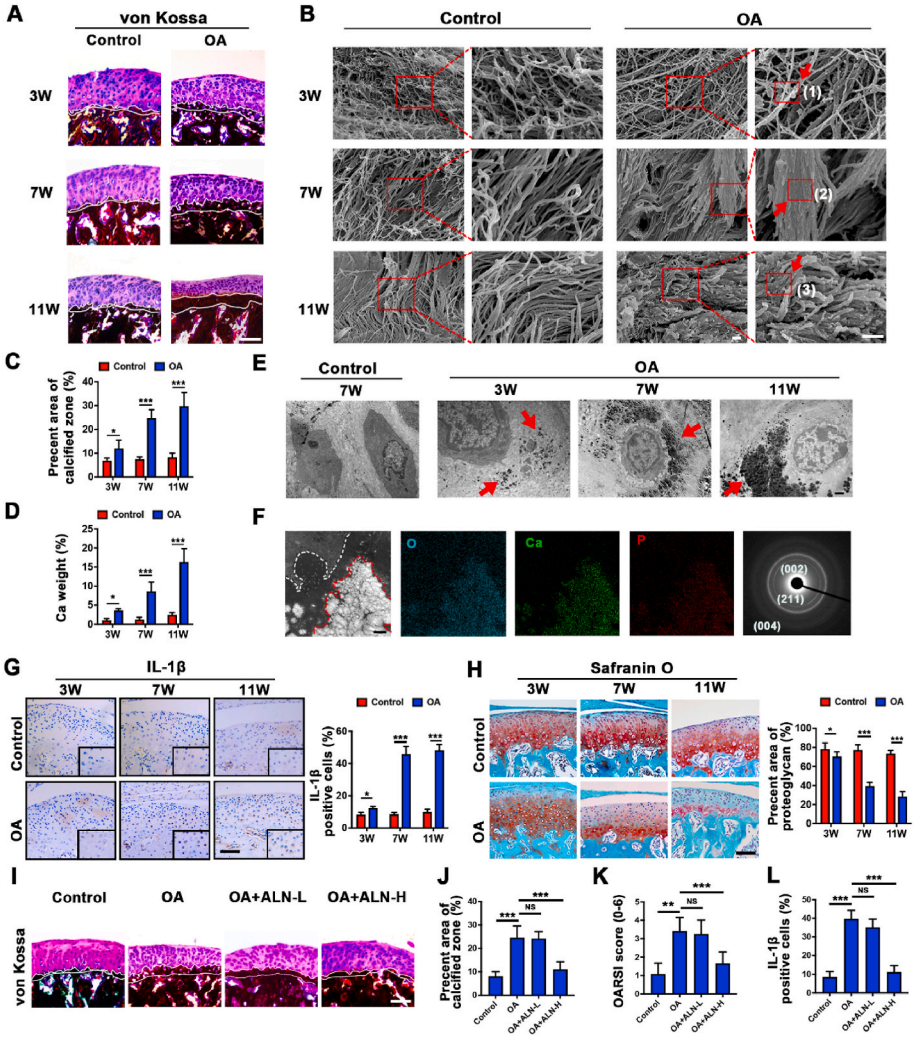

Fig. 1. Hydroxyapatite deposition was associated with IL-1β expression and cartilage degeneration. A) von Kossa and hematoxylin & eosin co-staining of sagittal central sections of the temporomandibular joint (TMJ) from the 3-, 7- and 11-week control and osteoarthritis (OA) groups. Areas stained black within the white lines indicated calcified cartilage zone. Scale bar: 100 μm. **B)** SEM images of the cartilage derived from the control and OA groups. Scale bar: 400 nm. High magnification of the areas depicted by the red rectangles showed calcified particulates and mineralized deposits (red arrows). Scale bar: 400 nm. **C)** Quantitative analysis of the percentage area of calcified cartilage to whole cartilage in (A) (n = 6). **D)** Quantitative analysis of calcium element distribution in the cartilage in (B) (n = 6). **E)** Representative TEM images of the extracellular matrix of cartilage specimen derived from the 7-week control group and OA groups. Red arrows indicated the mineral deposits in the extracellular matrix. Scale bar: 1 μm. **F)** Elemental mapping and selected area electron diffraction (SAED) of the mineral deposits in the extracellular matrix of a 7-week osteoarthritic cartilage specimen. The chondrocyte was within dotted white lines while the area within dotted red lines was used for SAED test (the left panel). SAED patterns showing diffraction rings corresponding to (002), (211), (004) crystallographic planes of hydroxyapatite (the right panel). O: oxygen (blue), Ca: calcium (green), P: phosphorus (red). Scale bar: 1 μm. **G)** Immunochemical staining of IL-1β protein and quantitative analysis of the percentage of the IL-1β-positive chondrocyte in sagittal central sections of the TMJ from the control and OA groups. **H)** Safranin O staining and quantitative analysis of the percentage of the area of proteoglycans to whole cartilage in sagittal central sections of the TMJ from the control and OA groups. **I)** von Kossa and hematoxylin & eosin co-staining of sagittal central sections of the TMJ from different groups. OA + ALN-L: osteoarthritis with low dose of alendronate (0.1 mg/kg); OA + ALN-H: osteoarthritis with high dose of alendronate (1 mg/kg). Scale bar: 100 μm. **J-L)** Quantitative analysis of the percentage area of calcified cartilage, the OARSI score and the percentage of IL-1β-positive chondrocytes in cartilage of (I), (S2E) and (S2F) respectively (n = 6). Statistical analyses in (C, D, G, H) were performed using two-way ANOVA with Holm-Šidák multiple comparison tests, while those in (J–L) were performed using one-way ANOVA with Holm-Šidák multiple comparison tests. NS, no significance; *, $P < 0.05$; **, $P < 0.01$; ***, $P < 0.001$.

inflammasomes [26]. To date, it is unknown whether these processes are involved in osteoarthritis.

Abnormal biomechanical stress is a key factor to the development of osteoarthritis [27,28]. The temporomandibular joint (TMJ), which relates biomechanically to dental occlusion, is one of the most frequent joints involved in osteoarthritis [29]. Accordingly, the animal TMJ-osteoarthritis model has been developed by the authors using unilateral anterior crossbite procedure to produce abnormal mechanical stress in TMJ, which exhibited cartilage degeneration, abnormal subchondral bone remodeling and early intra-cartilaginous mineral deposition [30–32]. In light of the aforementioned challenges, *in vitro* chondrocyte cultures and an *in vivo* murine TMJ-osteoarthritis model were used to investigate the contribution of hydroxyapatite in the progression of osteoarthritis, and to develop potential intervention strategies against pathological calcification in this highly debilitating disease. The overall hypothesis to be tested was that phagocytosis of extracellular hydroxyapatite crystallites produced during osteoarthritis by chondrocytes resulted in intracellular LMP and cytosolic release of CTSB that further activate NLRP3 inflammasomes to cause chondrocyte pyroptosis and cartilage degeneration.

2. Results

2.1. Effect of hydroxyapatite on IL-1β expression and cartilage degeneration

Cartilage calcification, a hallmark of osteoarthritis, could be visualized in the osteoarthritic cartilage as early as the 3rd week after von Kossa staining and Scanning electron microscopy (SEM) detection. Deterioration of it occurred at the 7th week and was substantial by the 11th week (Fig. 1A and B). Areas occupied by calcification were significantly increased in all osteoarthritic groups, compared with the control groups (Fig. 1C). SEM (Fig. 1B) and elemental mapping of the cartilage matrix (Figs. S1A–C) showed ample calcium-containing particulates in the vicinity of and along the collagen fibrils in the 3rd week osteoarthritic cartilage, which then aggregated into larger calcific plaques along the collagen fibrils at the 7th and 11th week. In contrast, calcification was not evident in the control groups (Fig. 1B). Accordingly, the relative amounts of calcium and phosphorus in the cartilage of the osteoarthritic groups were higher than those of the control groups at all time-points (Fig. 1D and Fig. S1D). Likewise, transmission electron microscopy (TEM) showed absence of mineral deposits in the cartilage collagen matrix of the control groups (Fig. 1E). In contrast, scattered mineral deposits were identified from the cartilage of the osteoarthritic group at the 3rd week; those deposits aggregated into larger mineral masses at the 7th and 11th week (Fig. 1E, red arrows). The results of elemental mapping and selected area electron diffraction (SAED) suggested the mineral in osteoarthritic cartilage was hydroxyapatite (Fig. 1F). Previous studies have identified hydroxyapatite was the main kind of mineral in osteoarthritic cartilage [11,33]. Similarly, in the present study, the Ca/P ratios of these minerals (Fig. S1E) and hydroxyapatite-characteristic vibration peaks (963, 1090, 1029, 3570 cm^{-1}) presented in osteoarthritic cartilage (Fig. S1F) indicated the hydroxyapatite was the main type of mineral in osteoarthritic cartilage. Simultaneously, the hydroxyapatite-characteristic P–O vibration peak at 1029 cm^{-1} was present in osteoarthritic cartilage while not in cartilage of control groups (Fig. S1G), suggesting the invasion of hydroxyapatite in cartilage during osteoarthritis progression. Atomic force microscopy (AFM) images further revealed characteristic D-band periodicity in the unmineralized collagen fibrils from the cartilage of control groups. This periodicity could no longer be discerned from the mineralized collagen fibrils in the osteoarthritic cartilage due to hydroxyapatite deposition within the fibrils (Fig. S1H). By the 7th and 11th weeks, the Young's modulus of the collagen matrix in the osteoarthritic groups were significantly increased, as determined by AFM (Fig. S1I).

Interleukin-1β is the major inflammatory protein in osteoarthritis. Apart from calcification, the amounts of this cytokine were significantly increased in the cartilage of all osteoarthritic groups (Fig. 1G and Fig. S1J). Cartilage degeneration was also evident in osteoarthritic mice, as manifested by the significant decrease in proteoglycans (Fig. 1H) and increase in the Osteoarthritis Research Society International (OARSI) histological score (Fig. S1K). The extent of calcification in the osteoarthritic cartilage was strongly correlated with IL-1β level (Fig. S1L, $r = 0.990$, $P = 0.0001$) and the OARSI score (Fig. S1M, $r = 0.979$, $P = 0.0006$).

Captivated by their strong correlations, inhibition of cartilage calcification was conducted to verify their causal relationship. Bisphosphonates is a stable pyrophosphate analog used for inhibition of ectopic mineralization [34]. As a bisphosphonate, high dose of alendronate has been used experimentally to prevent cartilage degeneration in osteoarthritic mice [35]. Subcutaneous injection of a high dose of alendronate significantly decreased hydroxyapatite deposition in the osteoarthritic cartilage, as revealed by von Kossa staining (Fig. 1I and J), SEM, elemental mapping (Figs. S2A–C) and Micro-Fourier transform infrared spectroscopy (Fig. S2D). At the same time, osteoarthritis severity (Fig. 1K, Figs. S2E and S2G) and IL-1β protein level (Fig. 1L, Figs. S2F and S2H) were reversed with the decrease in hydroxyapatite deposition. Despite the positive effects on alleviating osteoarthritis, high dose of alendronate severely decreased the body weight and humerus length of mice (Figs. S2I–J). While a low dose of alendronate for human use [36] did not influence all parameters mentioned above in osteoarthritic mice. The adverse effect of alendronate on bone development has been reported previously [37]. Collectively, the observations hinted that hydroxyapatite deposition within the osteoarthritic cartilage may be the cause of inflammation and cartilage degeneration.

2.2. The potential link between hydroxyapatite deposition and chondrocytes pyroptosis

Because NLRP3 inflammasomes play a critical role in IL-1β processing and pyroptosis [18,38,39], their activation of these entities in normal and osteoarthritic cartilage was further investigated. The percentage of NLRP3-positive chondrocytes was significantly increased in the osteoarthritic groups at the 7th and 11th weeks (Fig. 2A and C). Caspase1 p20 is the active form of Caspase1. As the indicator of NLRP3 inflammasome activation [18], the Caspase1 p20 level was significantly higher in the cartilage of osteoarthritic groups at the 7th and 11th weeks (Fig. 2B and D). Another function of NLRP3 inflammasome activation and Caspase1 production is the trigger of the canonical pathway of pyroptosis [18]. Images acquired using TEM showed evidence of pyroptotic morphology of the chondrocytes (ruptures in cell membranes and organelle destruction) in the highly calcified regions of osteoarthritic cartilages (Fig. 2E, red arrows). In addition, the percentages of dead chondrocytes (TUNEL-positive cells) and the protein levels of N-terminal gasdermin-D (N-GSDMD, the 'executor' of pyroptosis) were significantly increased in the osteoarthritic cartilages at 7th and 11th weeks (Fig. 2F–I and Figs. S3A–B), suggesting the increase of chondrocyte pyroptosis. However, with the decrease in hydroxyapatite deposition after high dose of alendronate application, NLRP3, Caspase1 p20, TUNEL and N-GSDMD-positive chondrocytes were also significantly decreased (Fig. 2J-O and Figs. S3C–D). These results are suggestive of a potential causal relationship between hydroxyapatite deposition and chondrocyte pyroptosis (Fig. 2P). But the exact mechanism needed to be further studied.

2.3. Mechanism whereby hydroxyapatite triggered chondrocyte pyroptosis

In vitro experiments were further conducted via co-culture of commercially available hydroxyapatite with chondrocytes to examine how hydroxyapatite induced chondrocyte pyroptosis (Fig. 3A). And the characterizations of the hydroxyapatite crystals were shown in Fig. S4.

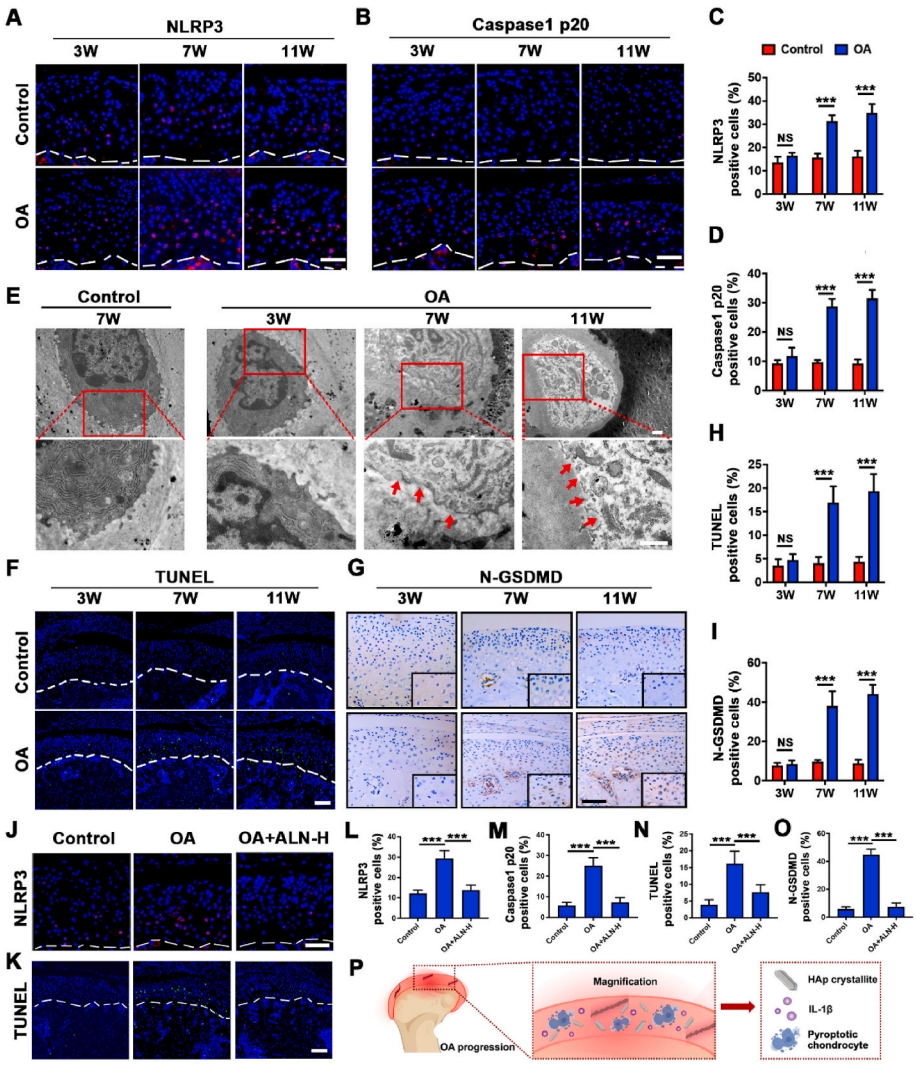

Fig. 2. Potential link between hydroxyapatite deposition and chondrocyte pyroptosis. A) Immunofluorescence staining of NLRP3 protein in the cartilage derived from different groups. NLRP3, red; DAPI, blue. Scale bar: 50 μm. **B)** Immunofluorescence staining of Caspase1 p20 protein in the cartilage derived from different groups. Caspase1 p20, red; DAPI, blue. Scale bar: 50 μm. **C-D)** Quantitative analysis of the percentage of NLRP3-positive and Caspase1 p20-positive chondrocytes in (A) and (B) respectively (n = 6). **E)** Representative TEM images of the cartilage specimens derived from the 7-week control group and osteoarthritis (OA) groups. The red arrows in magnified images indicated cell membrane ruptures. Scale bar: 1 μm. **F)** TUNEL staining of the cartilage derived from different groups. TUNEL, green; DAPI, blue. Scale bar: 100 μm. **G)** Immunochemical staining of N-GSDMD protein in the cartilage derived from different groups. Scale bar: 100 μm. **H–I)** Quantitative analysis of the percentage of TUNEL-positive and N-GSDMD-positive chondrocytes in (F) and (G) respectively (n = 6). **J)** Immunofluorescence staining of NLRP3 protein in the cartilage derived from different groups. NLRP3, red; DAPI, blue. OA + ALN-H: osteoarthritis with high dose of alendronate (1 mg/kg). Scale bar: 50 μm. **K)** TUNEL staining of the cartilage derived from different groups. TUNEL, green; DAPI, blue. Scale bar: 100 μm. **L-O)** Quantitative analysis of the percentage of NLRP3, Caspase1 p20, TUNEL and N-GSDMD-positive chondrocytes in (J), (S3C), (K) and (S3D) respectively. **P)** Schematic depicting the pathological changes in osteoarthritic cartilage from *in vivo* experiments. Statistical analyses in (C, D, H, I) were performed using two-way ANOVA with Holm-Šidák multiple comparison tests, while those in (L–O) were performed using one-way ANOVA with Holm-Šidák multiple comparison tests. NS, no significance; ***, $P < 0.001$. The dotted white lines in fluorescence staining images indicated the boundary of cartilage and subchondral bone.

The concentration of hydroxyapatite in osteoarthritic synovial fluid was reported to be between 20 and 100 μg/mL [40], and exposure of chondrocytes to 100 μg/mL hydroxyapatite for 24 h was identified as a suitable condition for inducing chondrocyte pyroptosis (Figs. S5A–D). These pyroptotic chondrocytes were featured by multiple ruptures of cell membranes (Fig. 3B, magnified images and red arrows), the swelling bubbles (Fig. S5E, red arrows) and accumulated N-GSDMD protein on plasm membranes (Fig. S5F) [41,42]. The levels of pyroptosis-related markers, NLRP3, Caspase1 p20, N-GSDMD (Fig. 3C and 3F–H) and IL-1β (Fig. 3I), were all significantly increased in chondrocytes that were co-cultured with hydroxyapatite. In addition, propidium iodide (PI)-positive cells (Fig. 3D–E) and lactate dehydrogenase (LDH) release (Fig. 3J) were also markedly elevated in chondrocytes that were exposed to hydroxyapatite, suggesting that the plasma membranes of those cells were ruptured and leaky. In addition, the decreased protein levels of collagen II and aggrecan (Fig. 3C and S5G-H) indicated the osteoarthritic change of chondrocytes.

Although the aforementioned results are suggestive of the role of hydroxyapatite in chondrocytes pyroptosis, additional inhibitory experiments are necessary to confirm the involvement of NLRP3 inflammasomes in hydroxyapatite-induced pyroptosis. Caspase1 is the downstream effector of NLRP3 inflammasomes for producing IL-1β and N-GSDMD [18]. Accordingly, VX-765 and MCC950 were used in the presence of hydroxyapatite, to inhibit the expression of Caspase1 and NLRP3 respectively [18]. Both VX-765 and MCC950 effectively reduced the protein levels of Caspase1 p20 induced by hydroxyapatite (Fig. 3C and G). These findings were indicative of successful inhibition of NLRP3 inflammasome activation. Silencing of NLRP3 inflammasomes reversed

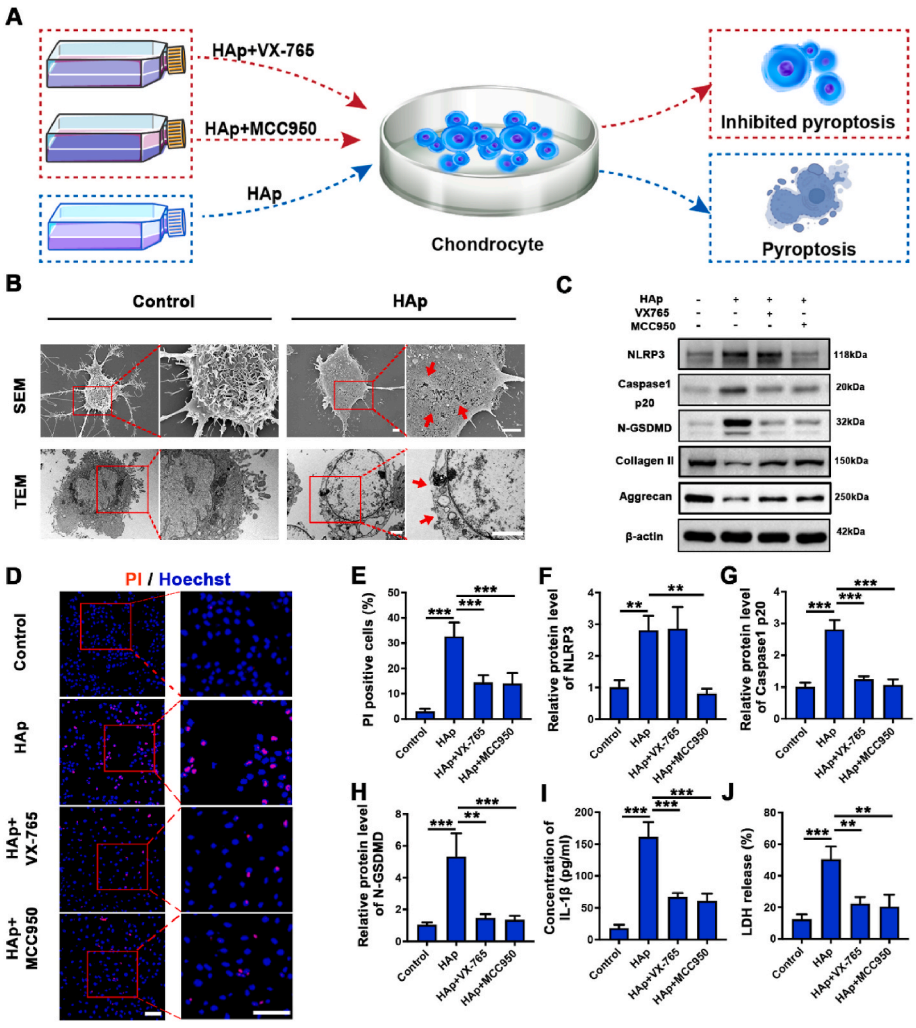

Fig. 3. Hydroxyapatite triggered chondrocyte pyroptosis via activation of NLRP3 inflammasome. A) Schematic depicting the design and results of the *in vitro* experiment. **B)** Representative SEM and TEM images of chondrocytes cultured with or without hydroxyapatite (HAp). Magnified images showed cell membrane pores and ruptures (red arrows). Scale bar: 2 μm. **C)** NLRP3, Caspase1 p20, N-GSDMD, collagen II and aggrecan protein levels of chondrocytes after the designated treatment, as determined by Western blot. **D)** Fluorescence co-staining of propidium iodide (PI) and Hoechst 33342 in chondrocytes of different groups. Scale bar: 100 μm. **E)** Quantitative analysis of the percentage of PI positive chondrocyte in (D) (n = 3). **F–H)** Quantitative analysis of NLRP3, Caspase1 p20 and N-GSDMD protein levels in (C) (n = 3). **I-J)** Quantitative analysis of IL-1β and lactate dehydrogenase (LDH) levels in chondrocyte culture supernatants in different groups (n = 3). Statistical analyses were performed using one-way ANOVA with Holm-Šidák multiple comparison tests. **, $P < 0.01$; ***, $P < 0.001$.

the protein levels of N-GSDMD (Fig. 3C and H) and IL-1β (Fig. 3I), as well as reduced the number of PI-positive cells (Fig. 3D–E) and LDH release (Fig. 3J). These observations were indicative of significant down-regulation of chondrocyte pyroptosis. Moreover, inhibition of pyroptosis also alleviated the osteoarthritic change of chondrocytes as the decreased collagen II and aggrecan protein levels caused by hydroxyapatite were reversed (Fig. 3C and S5G-H). Taken together, the series of experiments identified that hydroxyapatite induces chondrocytes pyroptosis via activation of NLRP3 inflammasomes. The overall result is deterioration of the osteoarthritic cartilage.

2.4. Intracellular events that occurred in chondrocytes after hydroxyapatite uptake

In the process of observing the pyroptotic chondrocytes by TEM *in vitro*, the hydroxyapatite crystallites were found to be phagocytized by chondrocytes (Fig. 4A), which was further confirmed by fluorescence staining (Fig. 4B). Besides, instead of irregular distribution, the internalized hydroxyapatite crystallites were mainly distributed in and processed by lysosomes (Fig. 4A and C). And the discontinuity in membranes of hydroxyapatite-loaded lysosomes was suggestive of LMP occurrence (Fig. 4A, red arrows). Lysosomal destabilization was reported involving NLRP3 inflammasome activation and cell death [43]. Therefore, *in vitro* and *in vivo* experiments were designed to clarify the way extracellular hydroxyapatite activates NLRP3 inflammasomes. Lysosensor staining is used for measuring the pH of lysosomes, it becomes more fluorescent in acidic environments to reflect their digestive function. The fluorescence intensity of this ratiometric probe was significantly decreased in chondrocytes of the hydroxyapatite-containing group, compared with that of control group (Figs. S6A and S6E). Simultaneously, the galectin-3 (Gal-3) puncta assay is a sensitive method for detection of LMP. Gal-3 protein migrates to and marks the leaky lysosomal membranes as LMP occurs [44]. Compared with the control group, there was a significant increase in the co-localization of Gal-3 with lysosome associated membrane protein 2 (LAMP2) in the hydroxyapatite-containing group (Fig. 4D–E). These results suggested that LMP of chondrocytes occurred in the presence of internalized hydroxyapatite.

After ascertaining that LMP was triggered by hydroxyapatite *in vitro*, an osteoarthritis animal model was used to examine whether this phenomenon also exists *in vivo*. TEM images of the osteoarthritic cartilages harvested at 7th and 11th weeks captured the phagocytosis of needle-

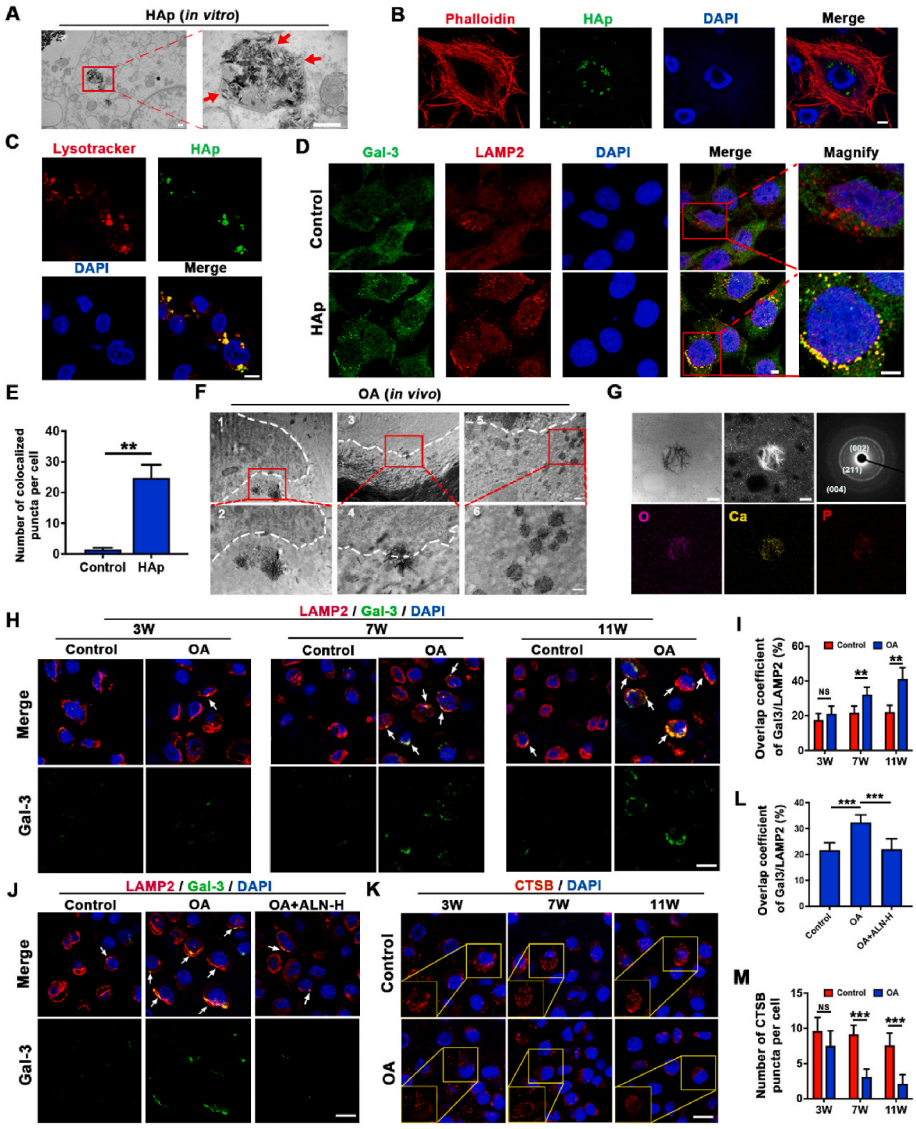

Fig. 4. Intracellular LMP and CTSB cytosolic release that occurred in chondrocytes after hydroxyapatite uptake. A) Representative TEM images of chondrocytes cultured with 100 μg/mL hydroxyapatite (HAp) for 24h. Scale bar: 300 nm. The magnified image showed HAp distribution in lysosomes. The discontinuity in lysosome membranes was indicated by red arrows. Scale bar: 300 nm. **B)** Fluorescence staining of rhodamine–phalloidin in chondrocytes cultured with 100 μg/mL fluorexon-labeled HAp for 6h. Scale bar: 10 μm. **C)** Fluorescence staining of lysotracker in living chondrocytes cultured with 100 μg/mL fluorexon-labeled HAp for 6h. Scale bar: 10 μm. **D)** Immunofluorescence co-staining of galectin-3 (Gal-3) and lysosome-associated membrane protein 2 (LAMP2) proteins in chondrocytes cultured with or without 100 μg/mL HAp. Scale bar: 5 μm. **E)** Quantitative analysis of the number of Gal-3 and LAMP2 co-localized puncta per cell in (D) (n = 3). **F)** Representative TEM images of chondrocytes in the cartilage specimen derived from the 7-week osteoarthritis (OA) groups. Magnified images show phagocytosis of crystallites in the chondrocytes. The dotted white lines represent the cell membranes. Scale bar: 500 nm. **G)** Elemental mapping and selected area electron diffraction (SAED) of the crystallites within the lysosomes of chondrocytes. SAED patterns showing diffraction rings corresponding to (002), (211), (004) crystallographic planes of HAp. O: oxygen (purple), Ca: calcium (yellow), P: phosphorus (red). Scale bar: 200 nm. **H)** Immunofluorescence co-staining of Gal-3 and LAMP2 proteins in the cartilage derived from different groups. Upper panel: merged images; Lower panel: single-channel images of Gal-3. Scale bar: 10 μm. **I)** Quantitative analysis of the Manders's coefficients for co-localization of Gal-3 and LAMP2 in (H) (n = 6). **J)** Immunofluorescence co-staining of Gal-3 and LAMP2 proteins in the cartilage derived from different groups. OA + ALN-H: osteoarthritis with high dose of alendronate (1 mg/kg). Upper panel: merged images; Lower panel: single-channel images of Gal-3. Scale bar: 10 μm. **K)** Immunofluorescence staining of cathepsin B (CTSB) protein in cartilage derived from different groups. Inset: single-channel images of CTSB. Scale bar: 10 μm. **L)** Quantitative analysis of the Manders's coefficients for co-localization of Gal-3 and LAMP2 in (J) (n = 6). **M)** Quantitative analysis of the number of CTSB puncta per chondrocyte in (K) (n = 6). Statistical analyses were performed using Student's t-test in (E), two-way ANOVA with Holm-Šidák multiple comparison tests in (I and M), and one-way ANOVA with Holm-Šidák multiple comparison tests in (L). NS, no significance; **, $P < 0.01$; ***, $P < 0.001$.

like mineral crystallites by chondrocytes. The crystallites initially clustered around the chondrocytes (Figs. 4F–1, 2), partially entered the cells (Figs. 4F–3, 4), and were eventually completely internalized by the cells (Figs. 4F–5, 6). The internalized crystallites were gathered in highly electron-dense intracellular organelles (Figs. 4F–6) with single membrane structure and around 1 μm in diameter (Fig. S6B), which conformed to the characters of lysosomes [45]. Discontinuity in the membrane of those lysosomes suggested the occurrence of LMP (Fig. S6B, red arrows). Elemental mapping and SAED further confirmed that the internalized crystallites were hydroxyapatite (Fig. 4G and S6C). The overlap coefficients of Gal-3 and LAMP2 in the osteoarthritic cartilages at 7th and 11th weeks were significant increased (Fig. 4H and I), confirming the occurrence of LMP within the osteoarthritic chondrocytes. In contrast, reduction in hydroxyapatite deposition in the osteoarthritic cartilage after high dose of alendronate treatment was also accompanied with significant decrease in Gal-3 and LAMP2 overlap

coefficients in the chondrocytes (Fig. 4J and L), indicating the recovery of LMP. These findings definitively affirmed that hydroxyapatite crystallites were the main cause of LMP within the osteoarthritic chondrocytes.

LMP activates NLRP3 inflammasomes via the release of CTSB into the cytosol [26]. The CTSB within the chondrocytes in the control groups had a granular appearance both *in vivo* (Fig. 4K) and *in vitro* (Fig. S6D) because the normal lysosomal membrane acts as a barrier that encloses the lysosomal enzymes. In contrast, the CTSB with red fluorescence appeared diffused within chondrocytes of the experimental groups (Fig. 4K and S6D). This is because the CTSB leaked into cytosol after damage of the lysosomal membrane. Quantitatively, this was reflected by a significant increase in the number of CTSB puncta per cell in the control groups *in vivo* (Fig. 4M) and *in vitro* (Fig. S6F). Moreover, the increased cytosolic level of CTSB in chondrocytes of experimental group was also confirmed by ELISA detection (Fig. S6G). Taken together, results of the *in vitro* and *in vivo* experiments confirmed that phagocytosis of hydroxyapatite resulted in LMP and cytosolic release of CTSB in the chondrocytes of osteoarthritic cartilage.

2.5. Role of cytosolic CTSB in chondrocytes pyroptosis

To confirm the role of cytosolic CTSB in chondrocyte pyroptosis induced by hydroxyapatite, small interfering RNA targeting CTSB (si-CTSB) was used to transfect chondrocyte and efficiently decreased the protein level of CTSB (Fig. 5A, C and 5E). As shown, si-CTSB also significantly decreased the protein levels of NLRP3 (Fig. 5B and F) and Caspase1 p20 (Fig. 5B and G), indicating that the hydroxyapatite induced NLRP3 inflammasome activation was inhibited. In addition, si-CTSB retarded the downstream chondrocytes pyroptosis as evidenced by decreased protein levels of N-GSDMD (Fig. 5B and H) and IL-1β (Fig. 5I), as well as the reduction of LDH level (Fig. 5J) and PI-positive cells (Fig. 5D and K).

Then, the efficacy of CA074me, a CTSB inhibitor [46], on eliminating the hydroxyapatite induced NLRP3 inflammasome activation and chondrocyte pyroptosis was also verified for selecting a potential therapeutic agent for *in vivo* inhibitory experiment. After CA074me application, Western blot showed that the protein expression of cytosolic CTSB was notably reduced (Fig. 5L and S7A), and the immunofluorescent staining demonstrated that the co-localization of Gal-3 with LAMP2 was also significantly decreased (Figs. S7B and S7C). These findings supported the efficacy of CA074me in inhibiting CTSB expression and alleviating LMP as previously reported [47]. In addition, the decreased cytosolic CTSB also effectively suppressed the development of hydroxyapatite induced NLRP3 inflammasome activation and chondrocytes pyroptosis, as revealed by the reduced protein levels of NLRP3

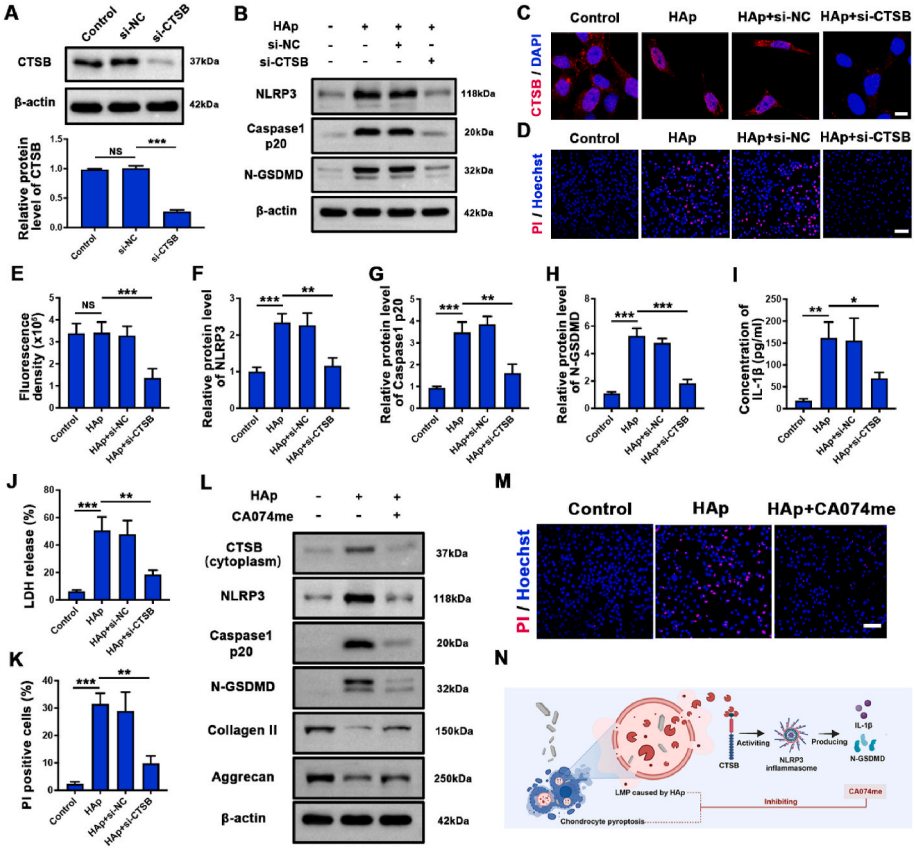

Fig. 5. Hydroxyapatite induced cytosolic CTSB contributed to NLRP3 inflammasome activation and caused chondrocyte pyroptosis. A) The Western blot result and quantitative analysis of Cathepsin B (CTSB) protein level of chondrocytes after transfected with siRNA targeting CTSB (si-CTSB). **B)** NLRP3, Caspase1 p20 and N-GSDMD protein levels of chondrocytes after the designated treatment, as determined by Western blot. **C)** Immunofluorescence staining of CTSB protein in chondrocytes of different groups. Scale bar: 10 μm. **D)** Fluorescence co-staining of propidium iodide (PI) and Hoechst 33342 in chondrocytes of different groups. Scale bar: 100 μm. **E)** Quantitative analysis of the fluorescence intensity of CTSB protein in (C) (n = 3). **F–H)** Quantitative analysis of NLRP3, Caspase1 p20 and N-GSDMD protein levels in (B) (n = 3). **I-J)** Quantitative analysis of IL-1β and lactate dehydrogenase (LDH) levels in chondrocyte culture supernatants of different groups (n = 3). **K)** Quantitative analysis of the percentage of PI-positive chondrocytes in (D) (n = 3). **L)** Cytosolic CTSB protein level and total NLRP3, Caspase1 p20, N-GSDMD, collagen II and aggrecan protein levels of chondrocytes after the designated treatment, as determined by Western blot. **M)** Fluorescence co-staining of PI and Hoechst 33342 in chondrocytes of different groups. Scale bar: 100 μm. **N**) Schematic depicting the mechanism whereby hydroxyapatite (HAp) triggered chondrocyte pyroptosis. Statistical analyses were performed using one-way ANOVA with Holm-Šidák multiple comparison tests. NS, no significance; *, $P < 0.05$; **, $P < 0.01$; ***, $P < 0.001$.

(Fig. 5L and S7D), Caspase1 p20 (Fig. 5L and S7E), N-GSDMD (Fig. 5L and S7F) and IL-1β (Fig. S7G), as well as the reduction in the propensity of PI-positive chondrocytes (Fig. 5M and S7H) and LDH release (Fig. S7I). Subsequently, CA074me also reversed the osteoarthritic changes of chondrocytes caused by hydroxyapatite, which was demonstrated by the significantly increased protein levels of collagen II and aggrecan (Fig. 5L and S7J-K). These changes caused by si-CTSB and CA074me confirmed that the hydroxyapatite induced LMP and subsequent cytosolic release of CTSB are the key mediator of NLRP3 inflammasome activation and chondrocyte pyroptosis (Fig. 5N).

Besides, it was reported that the calcium-containing crystals stimulate cells through 2 major mechanisms: directly activating cells after phagocytosis, or interaction between cell membrane and bound proteins on the crystal surface [48]. To clarify the main mechanism of the present study, cytochalasin D [25] was used to inhibit chondrocyte phagocytosis without disturbing the interaction between the adsorbed proteins and cell membrane. Consequently, Cytochalasin D efficiently inhibited the phagocytosis of hydroxyapatite crystals by chondrocytes (Fig. S8A), which alleviated the LMP (Figs. S8B–C) and cytosolic release of CTSB (Figs. S8D–E). Moreover, the activation of NLRP3 inflammasome and expression of pyroptotic markers in chondrocytes were all significantly inhibited by cytochalasin D (Fig. S8D and S8F-J). This finding indicated that the phagocytosis of crystals was the main cause of hydroxyapatite-induced pathological effects, and further confirmed the critical role of LMP and cytosolic CTSB in NLRP3 inflammasome dependent chondrocytes pyroptosis.

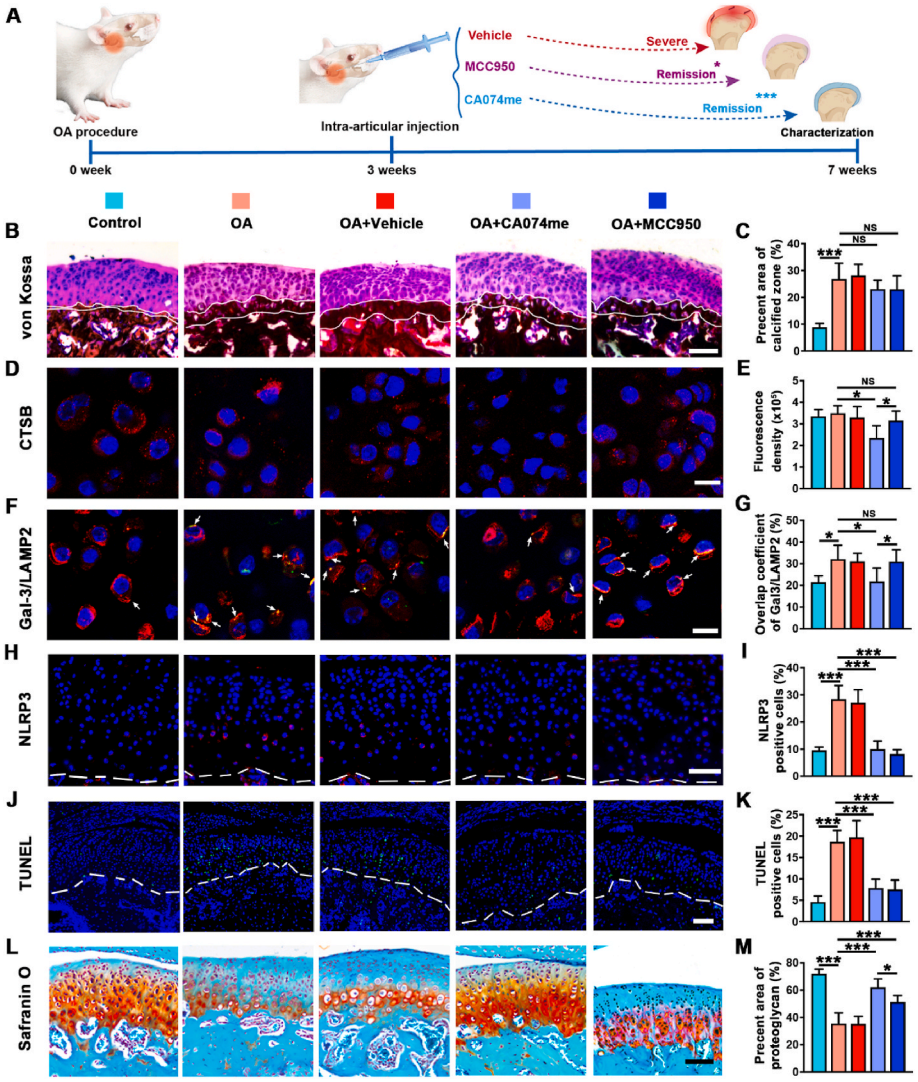

Fig. 6. Alleviation of LMP and inhibition of CTSB represented potential therapeutic targets in the management of experimental osteoarthritis. A) Schematic depicting the design and results of the *in vivo* experiment. **B)** von Kossa and hematoxylin & eosin co-staining in the cartilage derived from different groups. The areas between the white lines indicated calcified cartilage. Scale bar: 100 μm. **C)** Quantitative analysis of the percentage of calcified cartilage to whole cartilage in (B) (n = 6). **D)** Immunofluorescence staining of CTSB protein in cartilage derived from different groups. CTSB, red; DAPI, blue. Scale bar: 10 μm. **E)** Quantitative analysis of fluorescence intensity of CTSB in (D) (n = 6). **F)** Immunofluorescence co-staining of galectin-3 (Gal-3) and lysosome-associated membrane protein 2 (LAMP2) proteins in cartilage derived from different groups. The white arrows indicated the Gal-3 and LAMP2 colocalized area. Gal-3, green; LAMP2, red; DAPI, blue. Scale bar: 10 μm. **G)** Quantitative analysis of the Manders's coefficients for co-localization of Gal-3 and LAMP2 in (F) (n = 6). **H)** Immunofluorescence staining of NLRP3 protein in cartilage derived from different groups. NLRP3, red; DAPI, blue. Scale bar: 50 μm. **I)** Quantitative analysis of the percentage of NLRP3-positive chondrocytes in (H) (n = 6). **J)** Fluorescence staining of TUNEL in cartilage derived from different groups. TUNEL, green; DAPI, blue. Scale bar: 100 μm. **K)** Quantitative analysis of the percentage of TUNEL-positive chondrocytes in (J) (n = 6). **L)** Safranin O staining in cartilage derived from different groups. Scale bar: 100 μm. **M)** Quantitative analysis of the percentage of proteoglycans-positive area to whole cartilage in (L) (n = 6). Statistical analyses were performed using one-way ANOVA with Holm-Šidák multiple comparison tests. NS, no significance; *, $P < 0.05$; **, $P < 0.01$; ***, $P < 0.001$. The dotted white lines in fluorescence staining images indicated the boundary of cartilage and subchondral bone.

2.6. An experimental therapeutic regime for the management of osteoarthritis

Based on the results of the previous experiments, for alleviating osteoarthritis, CTSB and NLRP3 inflammasomes were used as potential therapeutic targets to countering the pathogenic effects of hydroxyapatite. Osteoarthritis was firstly inducted for 3 weeks to ensure sufficient deposition of hydroxyapatite within the cartilage. Then, the CTSB inhibitor CA074me and a specific NLRP3 inhibitor MCC950 were respectively delivered via intra-articular injection into the temporomandibular joints of osteoarthritic mice for 4 weeks (Fig. 6A). Consequently, both CA074me and MCC950 did not influence the deposition of intra-cartilaginous hydroxyapatite (Fig. 6B–C). In the presence of hydroxyapatite crystallites, CA074me significantly decreased the expression of CTSB and alleviated the occurrence of LMP in osteoarthritic cartilage, as revealed by the significant decreased fluorescence intensity of CTSB (Fig. 6D–E) and overlap coefficients of Gal-3 and LAMP2 (Fig. 6F–G) in the cartilage of CA074me treated osteoarthritic group than those in the osteoarthritic group. But MCC950 treatment did not affect the CTSB expression and LMP. Even so, each drug was capable of significantly inhibiting the hydroxyapatite induced activation of NLRP3 inflammasome as well as chondrocyte pyroptosis within the corresponding osteoarthritic cartilage. The inhibitory effects were supported by the significant reduction in the protein levels of NLRP3 (Fig. 6H–I), Caspase1 p20 (Figs. S9A and S9D), N-GSDMD (Figs. S9B and S9E) and IL-1β (Fig. S9C and S9F-G), as well as the significantly reduced percentages of dead chondrocytes (TUNEL-positive, Fig. 6J–K). Based on the OARSI score (Fig. S9H) and proteoglycan content (Fig. 6L-M), these two inhibitors notably halted cartilage destruction in the osteoarthritis model. Nevertheless, the efficacy for delaying osteoarthritis progression showed discrepancy between the two agents. CA074me obtained a better outcome than MCC950, which was indicated by lower OARSI score (Fig. S9H) and the presence of more proteoglycans in the cartilage of CA074me treated osteoarthritic group (Fig. 6L-M).

3. Discussion

Pathological calcification is well-established in osteoarthritic cartilage [10,12]. Intra-articular deposition of hydroxyapatite crystallites occurs in up to 70 % of osteoarthritis cases and is strongly correlated with the severity of cartilage degeneration [11,13,49]. Unfortunately, cartilage calcification is invariably present when osteoarthritis is diagnosed. This is because both the diagnostic schemes for osteoarthritis and detection methods for calcification are insensitive in clinical practice [50,51]. Although anti-calcification protocols have been reported, these protocols are mostly tested in animal models of cardiovascular and renal calcifications. The effects of these protocols on osteoarthritic calcification are controversial because of their inconsistent outcomes in different osteoarthritis animal models and their unpredictable side effects on skeletal development [12,37]. These problems were also experienced in the present work. Although a high dose of the bisphosphonate drug alendronate could reduce hydroxyapatite deposition in the osteoarthritic cartilage and reverse osteoarthritis progression, application of alendronate resulted in the loss of body weight and retarded elongation of the humerus (Fig. 1I-L and Fig. S2). To date, no infallible clinical technique is available to eliminate the hydroxyapatite deposition in osteoarthritis [11]. And the exact mechanisms in which intra-cartilaginous hydroxyapatite initiates inflammation and aggravates osteoarthritis are still controversial. These clinical challenges emphasize the urgency in unraveling how hydroxyapatite influences the osteoarthritis progression.

Hydroxyapatite found in the osteoarthritic cartilage is a type of basic calcium phosphate (BCP) crystallites with a size of 20–100 nm [51], which is the main kind of mineral in osteoarthritic cartilage [11]. Other endogenous or exogenous nanoscale crystals, such as monosodium urate in gout or silica in silicosis, activate NLRP3 inflammasomes to expedite inflammation and accelerate disease progression [21,22]. Incidentally, NLRP3 has been identified as a biomarker for diagnosing osteoarthritis [19]. Although pyroptosis induced by NLRP3 inflammasomes is responsible for the degradation of osteoarthritic cartilage, the activating mechanism of these inflammasomes is not comprehensively understood [52]. To shed light on these important issues, using *in vivo* and *in vitro* experiments, the present work clearly demonstrated that extracellular hydroxyapatite crystallites derived from osteoarthritic cartilages are an effective agonist for NLRP3 inflammasomes, which can instigate chondrocyte pyroptosis via activating intracellular NLRP3 inflammasomes after the crystallites are phagocytized by chondrocytes (Figs. 1–3). Because pyroptosis is a type of pro-inflammatory cell death, these results provide an explanation on why abnormal accumulation of hydroxyapatite can provoke acute arthritis, and why this phenomenon is related to the Milwaukee shoulder syndrome, a disease characterized by rapid and extensive cartilage destruction [14]. Moreover, as the NLRP3 inflammasome induced chondrocytes pyroptosis and IL-1β production simultaneously in the present study. And chondrocytes death is the core pathological event of osteoarthritis, which would deplete the source and disturb the remodeling of cartilage matrix due to their limited metabolic and proliferated activity. Therefore, pyroptosis may partially account for the undesired effectiveness of IL-1β inhibition in osteoarthritis treatment of human clinical trials.

Lysosomes are ubiquitous membrane-bound intracellular organelles with an acidic milieu. They are indispensable for degradation and recycling of cellular wastes [24]. In contrast to the rather simplified view of lysosomes as ‘waste bags’, lysosomes are recognized today as advanced organelles involved in many cellular processes and are considered crucial regulators of cell homeostasis [53]. Destabilization of lysosomes contributes to the development of diseases such as tumor, Alzheimer’s disease, and atherosclerosis. Control of lysosome quality has been regarded as a novel target for the treatment of these diseases [54]. Previous studies reported the phenomenon of lysosomal destabilization in osteoarthritic cartilage, in conjunction with elevation of the CTSB protein level [55,56]. However, the pathological link between lysosomal destabilization and osteoarthritis did not receive enough attention. The present work addresses this issue by identifying that the hydroxyapatite crystallites phagocytized by chondrocyte are the cause of lysosomal destabilization, which is featured by LMP and cytosolic release of CTSB (Fig. 4). The cytosolic CTSB, in turn, is the key for triggering NLRP3 inflammasome activation and chondrocyte pyroptosis that results in osteoarthritis progression (Figs. 5 and 6). Although previous researches of Klück V and Pazár B have both shown the BCP crystals in the form of hydroxyapatite could induce IL-1β expression of monocyte/macrophage via activating NLRP3 inflammasome, no experiments pointed out how the extracellular hydroxyapatite activated the intracellular NLRP3 inflammasomes [48,57]. The present work for the first time identified the critical role of intra-cartilaginous hydroxyapatite induced lysosomal destabilization in the pathogenesis of osteoarthritis, in which lysosomes serve as sensing organelle to turn the extracellular crystals into intracellular amplified dangerous signals leading to violent chondrocyte response of pyroptosis. Although hydroxyapatite induced LMP was observed both *in vivo* and *in vitro*, how it damages lysosomes remains unclear. LMP often occurs after prolonged exposure to stimuli such as oxygen free radicals and optical damage [54]. The authors speculate that the hydroxyapatite crystallites phagocytized by the chondrocytes have exceeded the digestive capability of the lysosomes, resulting in continuous irritation of these organelles. Our previous work identified that $LC3^{+}$ vesicles derived from secretory autophagy initiated hydroxyapatite formation during the early stage of osteoarthritis [58]. Results from the present work further demonstrated how the hydroxyapatite crystallites aggravated the progression of osteoarthritis. Autophagic activities, which are dependent on the digestion of lysosomes, have been reported to increase significantly during the early stage of osteoarthritis, and gradually decrease as osteoarthritis progresses [30]. Lysosomal destabilization caused by

gradually accumulation of intra-cartilaginous hydroxyapatite in the present study may account for the decrease in autophagic activity during the progression of osteoarthritis.

The goal of the present work was to propose feasible therapeutic targets for relieving osteoarthritis. Based on the hydroxyapatite-induced pathogenic pathway, potential therapeutic targets might include prevention of hydroxyapatite crystallite deposition, inhibition of chondrocyte phagocytosis, stabilization of lysosomes, or inhibition of NLRP3. To date, there is no effective means to prevent hydroxyapatite deposition or promote its dissolution [11]. Phagocytosis inhibition may disturb the physiological function of chondrocytes, such as nutrients acquisition and immune response [59,60]. Hence, the other two targets were selected for experimental treatment of osteoarthritis. The CTSB inhibitor CA074me has been reported to alleviate LMP and inhibit CTSB expression while MCC950 is a potent and specific inhibitor of NLRP3 inflammasome [47,61]. By intra-articular injection, both drugs inhibited NLRP3 inflammasome activation and chondrocyte pyroptosis and effectively retarding osteoarthritis progression. Surprisingly, CA074me demonstrated better efficacy than MCC950. In addition, CA074me alleviated the LMP and inhibited CTSB expression whereas MCC950 did not (Fig. 6). These differences may partially explain the discrepancy in their efficacies. Apart from activating NLRP3 inflammasomes, LMP may also influence other lysosomal functions. Release of CTSB into the cytosol may result in degradation of other essential cellular components, triggering detrimental effects other than pyroptosis [62]. Of note, although MCC950 has been highly esteemed in the pharmaceutical industry as the wonder drug for curing diseases such as osteoarthritis, a phase-II clinical trial of MCC950 has been suspended for the treatment of rheumatoid arthritis due to its hepatotoxicity. This adverse side effect indicates that MCC950 is unacceptable for clinical use [63]. These results supported that the LMP and cytosolic CTSB act as potential therapeutic targets of osteoarthritis.

Some limitations and perspectives of this work should be also presented. Firstly, although CA074me has been confirmed to inhibit LMP and CTSB efficiently in osteoarthritic chondrocytes, long-term intra-articular injection of the non-targeting agent may also disturb the physiological lysosomal functions of other cells such as fibroblast or macrophage of synovial tissue. This may result in potential side effects. Currently, the mesenchymal stem cell (MSC)-derived exsomes or extracellular vesicles (EVs) has been identified favoring cartilage homeostasis in osteoarthritis treatment [64,65]. Moreover, engineering, biomaterials modification, and gene editing techniques could endow them with improved functionality including targeted delivery [66–68]. Therefore, chondrocyte and lysosome targeted exsomes or EVs could be exploited to deliver LMP-modifying agents in osteoarthritis treatment. Secondly, similar to other biomaterials, hydroxyapatite crystals have the capacity to bind proteins from medium [69]. However, there is no effective technique to eliminate the binding proteins from biomaterials to date, making it is difficult to discern the detrimental effects of the present work are caused by the hydroxyapatite directly or by the proteins coating on them. This is a universal difficulty in studies of biomaterials. And further researches should pay more attention to the techniques for removing the binding proteins or other substances, which would make the results of relevant studies more accurate and convincing.

4. Conclusion

In conclusion, the present work reveals a previously unreported mechanism of cartilage calcification that results in cartilage degeneration in osteoarthritic joints. Lysosomal destabilization plays a central role in this mechanism. Hydroxyapatite crystallites deposited within the osteoarthritic cartilage are phagocytized by resident chondrocytes and processed by the lysosomes, resulting in LMP and CTSB release. The cytosolic CTSB activates NLRP3 inflammasomes, which, in turn, trigger chondrocyte pyroptosis and IL-1β production, resulting in the degeneration of osteoarthritic cartilage. Prevention of LMP and inhibition of CTSB release appear to be conceptual and promising targets for retarding osteoarthritis progression.

5. Materials and methods

5.1. Study design

The grouping designation and experimental scheme were illustrated in Fig. S10 of supplementary materials.

5.2. Murine osteoarthritis model and in vivo injection

Wild type female C57BL/6 J mice (6 weeks old, 20–25 g) were provided by the animal center of the Fourth Military Medical University. All experimental procedures, including the animal experiments, were approved by the Institutional Ethical Committee of Fourth Military Medical University (IACUC-20230024), according to the "Animal Research: Reporting of *In Vivo* Experiments" guidelines for preclinical animal studies. A unilateral anterior crossbite procedure was used to induce osteoarthritic-like changes in the murine temporomandibular joint (TMJ) cartilage of the mice [31]. Briefly, pinheads (Shinva Ande, Shandong, China) were used to form 1.5 mm-long metal tubes and 5 mm-long metal tubes. The shorter one was adhered to the left maxillary incisor with zinc phosphate cement. The longer one was bended at a 135° angle at the end of the tube and adhered to the left mandibular incisor. The mice in the control group were subjected to the same procedure but without fixation of a metal tube. In the experimental mice, no differences were noted in the manifestation of osteoarthritic phenotype between the right and left TMJ cartilage, as reported in the authors' previous work [31].

Mice in the alendronate injection group were injected subcutaneously with alendronate sodium trihydrate (A4798, MilliporeSigma, St Louis, MO, USA) 2 times per week. Injection started immediately after the induction of osteoarthritis until sacrifice of the mice at 7 weeks. As previously reported, the mouse in high dose alendronate (ALN-H) group received 1 mg/kg/dose alendronate dissolved in phosphate-buffered saline (PBS), while the mouse in low dose alendronate (ALN-L) group received 0.1 mg/kg/dose alendronate which is a dose for human use [35,36].

For TMJ injection, each mouse was laid sidewise after deep anesthesia with 1 % intraperitoneal sodium pentobarbital. A needle attached to a custom-designed Hamilton-type syringe was inserted just below the zygomatic arch between the corner of the eye and ear until the outer surface of the mandibular ramus was reached. The orientation of the needle head was adjusted to enable it to slide along the bone wall to reach the TMJ region. After induction of osteoarthritis for 3 weeks, 50 μL of 10 μM NLRP3 inhibitor MCC950 (HY-12815, MedChemExpress, New Jersey, USA), or 50 μL of 600 μM CTSB inhibitor CA074 me (S7420, Selleck, Pittsburgh, PA, USA) diluted in PBS was injected locally into the TMJ region of the injection groups. Injection was performed 2 times per week for 4 weeks [30].

5.3. Chondrocyte isolation and cell culture

Chondrocytes were isolated from the condylar cartilage of mouse TMJs by digestion with 0.25 % trypsin (MilliporeSigma, St. Louis, MO, USA) for 20 min. This was followed by digestion with 0.2 % type II collagenase (Invitrogen, ThermoFisher Scientific, Waltham, MA, USA) for 2–3 h [58]. The chondrocytes were grown to 70%–80 % confluence and serum-starved overnight in Dulbecco's Modified Eagle Medium/-Nutrient Mixture F-12 medium (DMEM/F12; Gibco, ThermoFisher Scientific) supplemented with 1 % penicillin/streptomycin (Invitrogen, ThermoFisher Scientific).

To investigate the role of hydroxyapatite on NLRP3 inflammasome activation and chondrocyte pyroptosis, nanoscale (particle size less than

100 nm) hydroxyapatite (H106378, Aladdin, Shanghai, China) at different concentrations (20-100μg/ml dissolved in DMEM/F12) were used to treat the chondrocytes for 12–24h. For pharmacological treatment, the Caspase 1 inhibitor VX-765 (HY-13205, MedChemExpress; 2.5 μM), NLRP3 inhibitor MCC950 (HY-12815, MedChemExpress; 1 μM), CTSB inhibitor CA074me (S7420, Selleck; 20 μM) and phagocytosis inhibitor cytochalasin D (HY–N6682, MedChemExpress; 200 nM) were used to treat chondrocytes for 1–2 h prior to the hydroxyapatite application, according to the design of respective experiments. Morphological images of chondrocytes were taken with a phase-contrast microscope (IX83, Olympus, Tokyo, Japan).

5.4. Small interfering RNA (siRNA) transfection

The siRNA targeting CTSB (si-CTSB) was purchased from Santa Cruz Biotechnology (sc-29933, Dallas, TX). To knockdown CTSB expression, chondrocytes were transfected with 50 nM si-CTSB for 24h with Lipofectamine 3000 reagent kit according to the manufacturer's protocols (Thermo Fisher Scientific, Waltham, MA). As a control, cells were transfected with sequence scrambled siRNA negative control (si-NC, sc-37007, Santa Cruz). Experiments were performed 24 h after transfection. Western blot and immunofluorescent staining were used to verify the efficacy of protein knockdown.

5.5. Histochemical, immunohistochemical and immunofluorescence staining

Pentobarbital overdose was performed to euthanize all mice. For each mouse, a tissue block that included the joint capsule and 3–4 mm of the tissue surrounding the condyle was harvested. After fixation in 4 % paraformaldehyde for 24 h and 30 % sucrose for 3 days, the specimens were embedded in optimal cutting temperature compound (Leica, Wetzlar, Germany) and stored at −80 °C. The tissue was cut into 5-μm thick sections. A cryofilm (Section-lab Co. Ltd., Hiroshima, Japan) was mounted onto the cut surface and the specimen was tightly adhered to the cryofilm. For von Kossa and hematoxylin-eosin co-staining, the cryofilm was stained with silver nitrate under the ultraviolet light for 1 min and rinsed with running water. The sections were subsequently stained with hematoxylin for 3 min and water-soluble eosin.

For immunofluorescence staining, the cryofilms were blocked with 1.5 % goat serum (MilliporeSigma) and individually incubated with primary antibodies. The primary antibodies used were: anti-NLRP3 (AG-20B-0014-C100, AdipoGen Corp., San Diego, CA, USA; diluted at 1:200), anti-Caspase1 p20 (AF4005, Affinity Bioscience, Cincinnati, OH, USA; diluted at 1:50), anti-LAMP2 (ab18528, Abcam, Cambridge, UK; diluted at 1:200), anti-Galectin-3 (60207-1-Ig, Proteintech, Wuhan, China; diluted at 1:400) and anti-cathepsin B (ab214428, Abcam; diluted at 1:250). The sections were incubated with secondary antibody (US Everbright Inc., Suzhou, China). After incubation, the sections were washed with PBS and the nuclei were counterstained with DAPI (Invitrogen).

For Safranin O/fast green and immunohistochemical staining, the tissue blocks were embedded in paraffin after fixation in 4 % paraformaldehyde for 24 h and decalcified in 10 % EDTA for 4 weeks. Four micrometer-thick serial sections were prepared through the TMJ in the sagittal plane. The sections were mounted on poly-L-lysine-coated glass slides. To perform Safranin O/fast green staining, the mounted sections were deparaffinized and stained with 0.02 % Fast Green for 2 min. The stained sections were rinsed with 1 % acetic acid solution, stained in 0.1 % safranin O solution for 5 min, and sequentially dehydrated with 95 % ethyl alcohol, absolute ethyl alcohol and xylene. As for immunohistochemical staining, the avidin-biotin complex (ABC) method was performed. After deparaffinization, hydration and blockage of endogenous peroxidase, the sections were incubated with goat serum to block special sites and then individually incubated with the respective primary antibody. The primary antibodies used were: N-GSDMD (DF13578, Affinity Bioscience; diluted at 1:50) and anti-IL-1β (2883818, Abcam; diluted at 1:400). After rinsing, the sections were incubated with biotinylated conjugated goat anti-rabbit secondary antibody, and then incubated with 3,3-diaminobenzidine tetrahydrochloride (DAB) substrate for 10 s to 2 min, depending on the requirement of the specific antibodies. Sections were mounted with balsam after being dehydrated in serial alcohol solutions. To ensure a reliable comparison between the specimens from different groups, the central sagittal sections of each joint were selected.

Histochemical and immunohistochemical images were taken with a light microscope (DM 2500, Leica, Wetzlar, Germany). Immunofluorescence images were taken with a confocal microscope (FV1000, Olympus, Tokyo, Japan). The percentage of immune-positive chondrocytes, percentage area of condylar cartilage with pathological calcification and Safranin O-positive area, the relative fluorescence intensity and fluorescence colocalization analysis were measured with Image J software (National Institute of Health, Bethesda, MD, USA) [70]. The OARSI score in the different groups was evaluated according to the histological results [32].

5.6. Scanning electron microscopy and energy-dispersive X-ray spectroscopy

Cartilage specimens and chondrocytes were fixed in 2.5 % glutaraldehyde in phosphate buffer (0.01 M, pH 7.4), washed extensively with water, dehydrated with an ascending series of ethanol (30–100 %) and treated with hexamethyldisilane (Electron Microscopy Sciences, Hatfield, PA, USA) that was slowly evaporated. The dried specimens were secured to sample holders with carbon tape and imaged with a field-emission scanning electron microscope (FE-SEM, S-4800, Hitachi, Tokyo, Japan) operated at 5 kV. Energy-dispersive X-ray spectroscopy (Element EDS System, Ametek, Berwyn, PA, USA) was used to characterize the mineral elemental composition in the cartilage.

5.7. Transmission electron microscopy

The cartilage specimens and chondrocyte were fixed in 2.5 % glutaraldehyde in phosphate buffer (0.01 M, pH = 7.4). The specimens were post-fixed in 1 % osmium tetroxide, dehydrated in an ascending series of ethanol, immersed in propylene oxide and embedded in epoxy resin. Ninety nanometer-thick sections were obtained, stained with uranyl acetate and Reynold's lead citrate, and observed using a JEM-123 transmission electron microscope (TEM, JEOL, Tokyo, Japan) at 110 kV.

5.8. Elemental mapping

Elemental mapping was performed by a scanning TEM (STEM) equipped with EDS to characterize the mineral elemental composition in the cartilage. Specimens used for elemental mapping were not post-fixed with osmium tetroxide to avoid interference during EDS. Unstained thin sections were examined with a Technai G2 STEM (FEI, Hillsboro, OR, USA) at 200 kV. Elemental mapping and selected area electron diffraction (SAED) were conducted using an INCA X-sight detector (Oxford Instruments, Abingdon, UK). Mappings were acquired with the FEI TIA software using a spot dwell time of 300 ms with drift correction performed after every 30 images.

5.9. Atomic force microscopy (AFM)

An AFM (Keysight 5500, Keysight Technologies, Santa Rosa, CA, USA) was used to analyze 20 μm thick fresh frozen tissue sections without decalcification. For the micromorphological imaging, after the sections were washed with water to remove the embedding medium (O.C.T compound) and dried naturally. A silicon probe (PPP-NCLR-20, Nanosensors™, Neuchatel, Switzerland) with a force constant of 42 N/m and a resonance frequency of 161 kHz was used for imaging. For

measurement of mechanical properties, the AFM-based nanoindentation was used. The washed specimens were immersed in physiological saline at room temperature, and a silicon oxide tip with 13 kHz resonance frequency and 0.2 N/m force constant (SD-Sphere-CONT-M-10, Nanosensors) was used in the contact mode. The elastic modulus of each position was measured at an indentation depth of 300 nm. All measurements were repeated for six positions in each tissue specimen, and the values were averaged.

5.10. Micro-Fourier transform infrared spectroscopy (Micro-FTIR)

The spotlight 400 m-FTIR imaging system (PerkinElmer, Inc., Waltham, MA, USA) was used to analyze the fresh frozen tissue sections without decalcification which were washed with water to remove the embedding medium (O.C.T compound) and dried naturally. The resolution of spectral acquisition was 4 cm^{-1}, ranging from 650 to 4000 cm^{-1}, and 36 scans were used for each sample. Spectrum software (PerkinElmer, Inc.) was used to obtain the absorption wavelengths.

5.11. Raman spectroscopy

Raman spectroscopy was carried out using Labram HR evolution (Horiba, Japan) with excitation at 633 nm from He–Ne laser at room temperature. Three separated locations were randomly chosen for repetitive scanning with spectral regions from 50 cm^{-1}–1800 cm^{-1}.

5.12. In vivo cell death detection

The terminal deoxynucleotidyl transferase-mediated deoxyuridine triphosphate nickend labeling (TUNEL) staining was performed with the *in situ* cell death detection kit (11684795910, Roche, Mannheim, Germany) for *in vivo* detection of chondrocyte death. After incubating with proteinase K, TUNEL reaction mixture solution was added at 37 °C for 1 h. Specimens were examined in the dark using a confocal microscope (FV1000, Olympus, Tokyo, Japan). Positive and negative controls were incubated with 0.01 mg/ml bovine pancreatic DNase I (10104159001, MilliporeSigma) or labeling solution respectively. The percentage of TUNEL-positive cells was calculated from the number of total cells using the Image J software.

5.13. In vitro cell viability assay

The viability of chondrocytes was determined using Cell Counting Kit-8 (C0043, Beyotime, Shanghai, China) according to the manufacturer's instructions. Briefly, cells were seeded in 96-well plates at a density of 5×10^3 cells/well and treated with commercially available hydroxyapatite (20, 50, 70 and 100 μg/mL) 12 or 24 h. The cells were washed twice with PBS prior to adding CCK-8 to each well. After further incubation for 1 h, the absorbance at 450 nm was evaluated using a microplate reader (Multi Skyhigh, Thermo Fisher Scientific).

5.14. Pyroptotic cell death assay (Hoechst 33342/PI and lactate dehydrogenase release)

To confirm pore formation in cell membranes, Hoechst 33342 and propidium iodide (PI) staining were performed. Chondrocytes were seeded on glass bottom dishes and grown to 70%–80 % confluence. After the designated treatment, the cells were incubated with a mixed solution of Hoechst 33342 and PI (P0137, Beyotime) for 30 min at 4 °C and photographed under a confocal fluorescence microscope. For lactate dehydrogenase (LDH) release, chondrocytes were seeded into 6-well plates overnight. After the indicated treatment, the cell culture supernatants were collected, and LDH release was measured using an LDH Cytotoxicity Kit (C20300, Invitrogen, ThermoFisher Scientific) and a microplate reader according to the manufacturer's instructions.

5.15. ELISA detection

For IL-1β level assay of cartilage, the dissected cartilage tissues were smashed into powder using our developed metal device in liquid nitrogen [30]. Then, the powder was lysed by RIPA buffer (Beyotime) containing protease inhibitor cocktail (Roche) immediately for total protein extraction. After determining the concentrations of proteins with a BCA protein kit (ThermoFisher Scientific), 100 μL protein solution from different groups were used for ELISA detection using a commercial mouse IL-1β assay kits (E-EL-M0037c, Elabscience) according to the manufacturer's instructions. And the protein level of IL-1β per mg of total protein was calculated. For IL-1β level assay in chondrocytes, the chondrocytes were seeded into 6-well plates grown to 70%–80 % confluence. After the indicated treatment, the cell culture supernatants were collected and IL-1β levels were determined by the same method.

For cytosolic CTSB level assay in chondrocytes, the cytosolic protein without disruption of lysosomes were extracted by a described digitonin extraction method [71]. After determining the concentrations of proteins with a BCA protein kit, 100 μL protein solution from different groups were used for ELISA detection using a commercial mouse CTSB assay kits (E-EL-M2423c, Elabscience) according to the manufacturer's instructions. And the protein level of CTSB per mg of total protein was calculated.

5.16. Cellular uptake of hydroxyapatite

Hydroxyapatite was labeled via fluorexon to explore cellular uptake. Briefly, 100 mg hydroxyapatite and 10 mL fluorexon solution (10 mg/mL) were mixed and stirred for 30min at room temperature. Then the hydroxyapatite crystals were then collected through centrifugation, washed several times with anhydrous ethanol and distilled water to ensure that no free fluorexon remained, and dried. After exposure of chondrocytes to 100 μg/mL fluorexon-hydroxyapatite for 6h, the cells were fixed with 4 % paraformaldehyde and stained with rhodamine–-phalloidin and DAPI and observed in the confocal microscope (FV1000, Olympus, Tokyo, Japan).

5.17. Immunofluorescence staining of cell culture

Chondrocytes were seeded on glass-bottom dishes grown to 70%–80 % confluence. After the designated treatment, the cells were washed using PBS three times before fixed by 4 % paraformaldehyde and then blocked with goat serum before individually incubated with primary antibodies. The primary antibodies used were: anti-LAMP2 (ab18528, Abcam; diluted at 1:200), anti-Galectin-3 (60207-1-Ig, Proteintech; diluted at 1:400) and anti-cathepsin B (ab214428, Abcam; diluted at 1:250). The sections were incubated with secondary antibody (US Everbright Inc., Suzhou, China). After incubation, the sections were washed with phosphate-buffered saline and the nuclei were counterstained with DAPI (Invitrogen). The immunofluorescence images were taken with the confocal microscope (FV1000, Olympus, Tokyo, Japan). Relative fluorescence intensity and fluorescence co-localization analysis were analyzed with Image J.

5.18. Lysotracker red and Lysosensor green staining

Chondrocytes were seeded on glass-bottom dishes grown to 70%–80 % confluence. After the designated treatment, the cells were washed twice with PBS and incubated for 30 min with 2 mL of pre-warmed medium containing LysoTracker Deep Red (L12492, Invitrogen, ThermoFisher Scientific, 75 nM) and Lysosensor Green DND-189 (L7535, Invitrogen, ThermoFisher Scientific, 75 nM) respectively according to the manufacturer's protocols. After washing with PBS, cells were viewed and imaged using a confocal fluorescence microscope (FV1000, Olympus, Tokyo, Japan). Relative fluorescence intensity was analyzed using Image J.

5.19. Western blot

The total protein of cartilage tissues were extracted by the same methods described in ELISA detection (5.15). For the total protein extraction of chondrocytes, the cells were lysed in RIPA buffer (Beyotime) containing protease inhibitor cocktail (Roche). For the extraction of cytosolic protein without disruption of lysosomes for detecting the CTSB protein level in cytoplasm, chondrocytes were lysed by a described digitonin extraction method [71]. Protein concentrations were quantified by using a BCA protein kit (ThermoFisher Scientific). Samples (30 μg protein per lane) were loaded on 12 % SDS-PAGE gels. After electrophoresis, the proteins were transferred to polyvinylidene fluoride membranes (MilliporeSigma). Then, the membranes were blocked with 5 % bovine serum albumin (BSA) and incubated at 4 °C overnight with the appropriate primary antibodies: anti-NLRP3 (ab263899, Abcam; diluted at 1:1000), anti-Caspase1 p20 (AF4005, Affinity Bioscience, diluted at 1:500), anti-N-GSDMD (DF13578, Affinity Bioscience; diluted at 1:500), anti-cathepsin B (ab214428, Abcam; diluted at 1:1000) and anti-Beta actin (66009-1-Ig, Proteintech). Immunoreactivity was detected by incubation with horseradish peroxidase-conjugated secondary antibodies (Invitrogen, 1: 5000) followed by WesternLumaxLight Sirius HRP substrate (310231, ZETA LIFE,CA,USA). Optical densities of the bands were calculated using Image J. All samples were run in parallel with three replicates.

5.20. Statistical analysis

Analyses were performed using GraphPad Prism 8.0 (GraphPad Software, San Diego, CA, USA). All data were presented as means ± standard deviations. The Shapiro-Wilk test and modified Leven test were used respectively to test the normality and homoscedasticity assumptions of the corresponding data sets. The Student's *t*-test, one-factor or two-factor analysis of variance (ANOVA) followed by Holm-Šidák multiple comparison tests were used to evaluate the differences among groups. Pearson correlation analysis was used to compare the correlation between different indexes. For all tests, statistical significance was preset at $\alpha = 0.05$.

Ethics approval and consent to participate

This work does not contain results related to human participant.

All experimental protocols in this work met the National Institute of Health guidelines for the care and use of laboratory animals, and were reviewed and approved by the Institutional Animal Care and Use Committee of the Fourth Military Medical University (IACUC-20230024). The following is the file of Ethics approval.

CRediT authorship contribution statement

Tao Ye: Conceptualization, Funding acquisition, Investigation, Methodology, Writing – original draft. **Chenyu Wang:** Methodology, Visualization, Writing – original draft. **Jianfei Yan:** Investigation, Methodology, Visualization. **Zixuan Qin:** Conceptualization, Formal analysis, Methodology. **Wenpin Qin:** Data curation, Investigation, Methodology. **Yuxuan Ma:** Data curation, Software. **Qianqian Wan:** Methodology, Visualization. **Weicheng Lu:** Data curation, Formal analysis, Methodology, Validation. **Mian Zhang:** Data curation, Formal analysis, Methodology. **Franklin R. Tay:** Conceptualization, Writing – original draft, Writing – review & editing. **Kai Jiao:** Conceptualization, Supervision, Writing – original draft. **Lina Niu:** Conceptualization, Supervision, Validation, Writing – original draft, Writing – review & editing.

Declaration of competing interest

The authors declare no conflict of interest.

Acknowledgments

This work was supported by National Natural Science Foundation of China (82001072, 81870805, 82170978), National Key R&D Program of China (2022YFC2405900, 2022YFC2405901), and the Shaanxi Key Scientific and Technological Innovation Team (2020TD-033).

Appendix A. Supplementary data

Supplementary data to this article can be found online at https://doi.org/10.1016/j.bioactmat.2023.12.001.

References

[1] M. Kapoor, J. Martel-Pelletier, D. Lajeunesse, J.P. Pelletier, H. Fahmi, Role of proinflammatory cytokines in the pathophysiology of osteoarthritis, Nat. Rev. Rheumatol. 7 (1) (2011) 33–42.
[2] F. Berenbaum, Osteoarthritis as an inflammatory disease (osteoarthritis is not osteoarthrosis!), Osteoarthritis Cartilage 21 (1) (2013) 16–21.
[3] J. Wu, H. Li, F. Hu, P. Luo, Stevioside attenuates osteoarthritis via regulating Nrf2/HO-1/NF-kappaB pathway, J. Orthop. Translat. 38 (2023) 190–202.
[4] B. Dai, Y. Zhu, X. Li, Z. Liang, S. Xu, S. Zhang, Z. Zhang, S. Bai, W. Tong, M. Cao, Y. Li, X. Zhu, W. Liu, Y. Zhang, L. Chang, P.S. Yung, K. Ki-Wai Ho, J. Xu, T. Ngai, L. Qin, Blockage of osteopontin-integrin beta3 signaling in infrapatellar fat pad attenuates osteoarthritis in mice, Adv. Sci. 10 (22) (2023), e2300897.
[5] C. Wen, G. Xiao, Advances in osteoarthritis research in 2021 and beyond, J. Orthop. Translat. 32 (2022) A1–A2.
[6] Q. Yao, X. Wu, C. Tao, W. Gong, M. Chen, M. Qu, Y. Zhong, T. He, S. Chen, G. Xiao, Osteoarthritis: pathogenic signaling pathways and therapeutic targets, Signal Transduct. Targeted Ther. 8 (1) (2023) 56.
[7] X. Chang, Y. Kang, Y. Yang, Y. Chen, Y. Shen, C. Jiang, Y. Shen, Pyroptosis: a novel intervention target in the progression of osteoarthritis, J. Inflamm. Res. 15 (2022) 3859–3871.
[8] L.H. Chang, C.H. Chen, S.C. Wu, J.K. Chang, M.L. Ho, Cyclooxygenase-2 regulates PTHrP transcription in human articular chondrocytes and is involved in the pathophysiology of osteoarthritis in rats, J. Orthop. Translat. 30 (2021) 16–30.
[9] X. Cao, Z. Cui, Z. Ding, Y. Chen, S. Wu, X. Wang, J. Huang, An osteoarthritis subtype characterized by synovial lipid metabolism disorder and fibroblast-like synoviocyte dysfunction, J. Orthop. Translat. 33 (2022) 142–152.
[10] J.F. Yan, W.P. Qin, B.C. Xiao, Q.Q. Wan, F.R. Tay, L.N. Niu, K. Jiao, Pathological calcification in osteoarthritis: an outcome or a disease initiator? Biol. Rev. Camb. Phil. Soc. 95 (4) (2020) 960–985.
[11] X. Wang, Q. Wu, R. Zhang, Z. Fan, W. Li, R. Mao, Z. Du, X. Yao, Y. Ma, Y. Yan, W. Sun, H. Wu, W. Wei, Y. Hu, Y. Hong, H. Hu, Y.W. Koh, W. Duan, X. Chen, H. Ouyang, Stage-specific and location-specific cartilage calcification in osteoarthritis development, Ann. Rheum. Dis. 82 (3) (2022) 393–402.
[12] I. Bernabei, A. So, N. Busso, S. Nasi, Cartilage calcification in osteoarthritis: mechanisms and clinical relevance, Nat. Rev. Rheumatol. 19 (1) (2023) 10–27.
[13] G.M. McCarthy, H.S. Cheung, Point: hydroxyapatite crystal deposition is intimately involved in the pathogenesis and progression of human osteoarthritis, Curr. Rheumatol. Rep. 11 (2) (2009) 141–147.
[14] C. Jin, P. Frayssinet, R. Pelker, D. Cwirka, B. Hu, A. Vignery, S.C. Eisenbarth, R. A. Flavell, NLRP3 inflammasome plays a critical role in the pathogenesis of hydroxyapatite-associated arthropathy, Proc. Natl. Acad. Sci. U.S.A. 108 (36) (2011) 14867–14872.
[15] Z. Jenei-Lanzl, A. Meurer, F. Zaucke, Interleukin-1beta signaling in osteoarthritis - chondrocytes in focus, Cell. Signal. 53 (2019) 212–223.
[16] X. Chevalier, F. Eymard, Anti-IL-1 for the treatment of OA: dead or alive? Nat. Rev. Rheumatol. 15 (4) (2019) 191–192.
[17] X. Chevalier, F. Eymard, P. Richette, Biologic agents in osteoarthritis: hopes and disappointments, Nat. Rev. Rheumatol. 9 (7) (2013) 400–410.
[18] K.V. Swanson, M. Deng, J.P. Ting, The NLRP3 inflammasome: molecular activation and regulation to therapeutics, Nat. Rev. Immunol. 19 (8) (2019) 477–489.
[19] M.J. McAllister, M. Chemaly, A.J. Eakin, D.S. Gibson, V.E. McGilligan, NLRP3 as a potentially novel biomarker for the management of osteoarthritis, Osteoarthritis Cartilage 26 (5) (2018) 612–619.
[20] T. Murakami, Y. Nakaminami, Y. Takahata, K. Hata, R. Nishimura, Activation and function of NLRP3 inflammasome in bone and joint-related diseases, Int. J. Mol. Sci. 23 (10) (2022).
[21] V. Hornung, F. Bauernfeind, A. Halle, E.O. Samstad, H. Kono, K.L. Rock, K. A. Fitzgerald, E. Latz, Silica crystals and aluminum salts activate the NALP3 inflammasome through phagosomal destabilization, Nat. Immunol. 9 (8) (2008) 847–856.
[22] F. Martinon, V. Pétrilli, A. Mayor, A. Tardivel, J. Tschopp, Gout-associated uric acid crystals activate the NALP3 inflammasome, Nature 440 (7081) (2006) 237–241.
[23] K. Shirasuna, T. Karasawa, M. Takahashi, Exogenous nanoparticles and endogenous crystalline molecules as danger signals for the NLRP3 inflammasomes, J. Cell. Physiol. 234 (5) (2019) 5436–5450.
[24] A. Ballabio, The awesome lysosome, EMBO Mol. Med. 8 (2) (2016) 73–76.
[25] P. Duewell, H. Kono, K.J. Rayner, C.M. Sirois, G. Vladimer, F.G. Bauernfeind, G. S. Abela, L. Franchi, G. Nuñez, M. Schnurr, T. Espevik, E. Lien, K.A. Fitzgerald, K.

L. Rock, K.J. Moore, S.D. Wright, V. Hornung, E. Latz, NLRP3 inflammasomes are required for atherogenesis and activated by cholesterol crystals, Nature 464 (7293) (2010) 1357–1361.
[26] M. Bruchard, G. Mignot, V. Derangere, F. Chalmin, A. Chevriaux, F. Vegran, W. Boireau, B. Simon, B. Ryffel, J.L. Connat, J. Kanellopoulos, F. Martin, C. Rebe, L. Apetoh, F. Ghiringhelli, Chemotherapy-triggered cathepsin B release in myeloid-derived suppressor cells activates the Nlrp3 inflammasome and promotes tumor growth, Nat. Med. 19 (1) (2013) 57–64.
[27] G. Zhen, Q. Guo, Y. Li, C. Wu, S. Zhu, R. Wang, X.E. Guo, B.C. Kim, J. Huang, Y. Hu, Y. Dan, M. Wan, T. Ha, S. An, X. Cao, Mechanical stress determines the configuration of TGFbeta activation in articular cartilage, Nat. Commun. 12 (1) (2021) 1706.
[28] T.M. Griffin, F. Guilak, The role of mechanical loading in the onset and progression of osteoarthritis, Exerc. Sport Sci. Rev. 33 (4) (2005) 195–200.
[29] S.J. Scrivani, D.A. Keith, L.B. Kaban, Temporomandibular disorders, N. Engl. J. Med. 359 (25) (2008) 2693–2705.
[30] H. Yang, Y. Wen, M. Zhang, Q. Liu, H. Zhang, J. Zhang, L. Lu, T. Ye, X. Bai, G. Xiao, M. Wang, MTORC1 coordinates the autophagy and apoptosis signaling in articular chondrocytes in osteoarthritic temporomandibular joint, Autophagy 16 (2) (2020) 271–288.
[31] M. Zhang, H. Wang, J. Zhang, H. Zhang, H. Yang, X. Wan, L. Jing, L. Lu, X. Liu, S. Yu, W. Chang, M. Wang, Unilateral anterior crossbite induces aberrant mineral deposition in degenerative temporomandibular cartilage in rats, Osteoarthritis Cartilage 24 (5) (2016) 921–931.
[32] J. Zhang, L. Liao, J. Zhu, X. Wan, M. Xie, H. Zhang, M. Zhang, L. Lu, H. Yang, D. Jing, X. Liu, S. Yu, X.L. Lu, C. Chen, Z. Shan, M. Wang, Osteochondral interface stiffening in mandibular condylar osteoarthritis, J. Dent. Res. 97 (5) (2018) 563–570.
[33] X. Wang, J. Lin, Z. Li, Y. Ma, X. Zhang, Q. He, Q. Wu, Y. Yan, W. Wei, X. Yao, C. Li, W. Li, S. Xie, Y. Hu, S. Zhang, Y. Hong, X. Li, W. Chen, W. Duan, H. Ouyang, Identification of an ultrathin osteochondral interface tissue with specific nanostructure at the human knee joint, Nano Lett. 22 (6) (2022) 2309–2319.
[34] G. Kranenburg, P.A. de Jong, J.W. Bartstra, S.J. Lagerweij, M.G. Lam, J. Ossewaarde-van Norel, S. Risseeuw, R. van Leeuwen, S.M. Imhof, H.J. Verhaar, J.J. de Vries, R. Slart, G. Luurtsema, A.M. den Harder, F.L.J. Visseren, W.P. Mali, W. Spiering, Etidronate for prevention of ectopic mineralization in patients with pseudoxanthoma elasticum, J. Am. Coll. Cardiol. 71 (10) (2018) 1117–1126.
[35] M.S. Khorasani, S. Diko, A.W. Hsia, M.J. Anderson, D.C. Genetos, D. R. Haudenschild, B.A. Christiansen, Effect of alendronate on post-traumatic osteoarthritis induced by anterior cruciate ligament rupture in mice, Arthritis Res. Ther. 17 (1) (2015) 30.
[36] E.D. Zhu, L. Louis, D.J. Brooks, M.L. Bouxsein, M.B. Demay, Effect of bisphosphonates on the rapidly growing male murine skeleton, Endocrinology 155 (4) (2014) 1188–1196.
[37] J.W. Vargas-Franco, B. Castaneda, F. Rédiní, D.F. Gómez, D. Heymann, F. Lézot, Paradoxical side effects of bisphosphonates on the skeleton: what do we know and what can we do? J. Cell. Physiol. 233 (8) (2018) 5696–5715.
[38] Y. Huang, W. Xu, R. Zhou, NLRP3 inflammasome activation and cell death, Cell. Mol. Immunol. 18 (9) (2021) 2114–2127.
[39] A. Grebe, F. Hoss, E. Latz, NLRP3 inflammasome and the IL-1 pathway in atherosclerosis, Circ. Res. 122 (12) (2018) 1722–1740.
[40] E.M. Corr, C.C. Cunningham, L. Helbert, G.M. McCarthy, A. Dunne, Osteoarthritis-associated basic calcium phosphate crystals activate membrane proximal kinases in human innate immune cells, Arthritis Res. Ther. 19 (1) (2017) 23.
[41] K. Wang, Q. Sun, X. Zhong, M. Zeng, H. Zeng, X. Shi, Z. Li, Y. Wang, Q. Zhao, F. Shao, J. Ding, Structural mechanism for GSDMD targeting by autoprocessed caspases in pyroptosis, Cell 180 (5) (2020) 941–955 e20.
[42] J. Ding, K. Wang, W. Liu, Y. She, Q. Sun, J. Shi, H. Sun, D.C. Wang, F. Shao, Pore-forming activity and structural autoinhibition of the gasdermin family, Nature 535 (7610) (2016) 111–116.
[43] F. Wang, R. Gomez-Sintes, P. Boya, Lysosomal membrane permeabilization and cell death, Traffic 19 (12) (2018) 918–931.
[44] S. Aits, J. Kricker, B. Liu, A.M. Ellegaard, S. Hamalisto, S. Tvingsholm, E. Corcelle-Termeau, S. Hogh, T. Farkas, A. Holm Jonassen, I. Gromova, M. Mortensen, M. Jaattela, Sensitive detection of lysosomal membrane permeabilization by lysosomal galectin puncta assay, Autophagy 11 (8) (2015) 1408–1424.
[45] H. Appelqvist, P. Waster, K. Kagedal, K. Ollinger, The lysosome: from waste bag to potential therapeutic target, J. Mol. Cell Biol. 5 (4) (2013) 214–226.
[46] X. Yang, Y. Wen, S. Liu, L. Duan, T. Liu, Z. Tong, Z. Wang, Y. Gu, Y. Xi, X. Wang, D. Luo, R. Zhang, Y. Liu, Y. Wang, T. Cheng, S. Jiang, X. Zhu, X. Yang, Y. Pan, S. Cheng, Q. Ye, J. Chen, X. Xu, S. Gao, LCDR regulates the integrity of lysosomal membrane by hnRNP K-stabilized LAPTM5 transcript and promotes cell survival, Proc. Natl. Acad. Sci. U.S.A. 119 (5) (2022).
[47] Y. Xu, J. Wang, X. Song, R. Wei, F. He, G. Peng, B. Luo, Protective mechanisms of CA074-me (other than cathepsin-B inhibition) against programmed necrosis induced by global cerebral ischemia/reperfusion injury in rats, Brain Res. Bull. 120 (2016) 97–105.
[48] B. Pazar, H.K. Ea, S. Narayan, L. Kolly, N. Bagnoud, V. Chobaz, T. Roger, F. Liote, A. So, N. Busso, Basic calcium phosphate crystals induce monocyte/macrophage IL-1beta secretion through the NLRP3 inflammasome in vitro, J. Immunol. 186 (4) (2011) 2495–2502.
[49] M. Fuerst, J. Bertrand, L. Lammers, R. Dreier, F. Echtermeyer, Y. Nitschke, F. Rutsch, F.K. Schafer, O. Niggemeyer, J. Steinhagen, C.H. Lohmann, T. Pap, W. Ruther, Calcification of articular cartilage in human osteoarthritis, Arthritis Rheum. 60 (9) (2009) 2694–2703.
[50] M. Camacho-Encina, V. Balboa-Barreiro, I. Rego-Perez, F. Picchi, J. VanDuin, J. Qiu, M. Fuentes, N. Oreiro, J. LaBaer, C. Ruiz-Romero, F.J. Blanco, Discovery of an autoantibody signature for the early diagnosis of knee osteoarthritis: data from the Osteoarthritis Initiative, Ann. Rheum. Dis. 78 (12) (2019) 1699–1705.
[51] P. MacMullan, G. McMahon, G. McCarthy, Detection of basic calcium phosphate crystals in osteoarthritis, Joint Bone Spine 78 (4) (2011) 358–363.
[52] S. An, H. Hu, Y. Li, Y. Hu, Pyroptosis plays a role in osteoarthritis, Aging. Dis. 11 (5) (2020) 1146–1157.
[53] J.P. Luzio, P.R. Pryor, N.A. Bright, Lysosomes: fusion and function, Nat. Rev. Mol. Cell Biol. 8 (8) (2007) 622–632.
[54] S.Y. Zhu, R.Q. Yao, Y.X. Li, P.Y. Zhao, C. Ren, X.H. Du, Y.M. Yao, Lysosomal quality control of cell fate: a novel therapeutic target for human diseases, Cell Death Dis. 11 (9) (2020) 817.
[55] M.Y. Ansari, H.C. Ball, S.J. Wase, K. Novak, T.M. Haqqi, Lysosomal dysfunction in osteoarthritis and aged cartilage triggers apoptosis in chondrocytes through BAX mediated release of Cytochrome c, Osteoarthritis Cartilage 29 (1) (2021) 100–112.
[56] A. Baici, A. Lang, R. Zwicky, K. Muntener, Cathepsin B in osteoarthritis: uncontrolled proteolysis in the wrong place, Semin. Arthritis Rheum. 34 (6 Suppl 2) (2005) 24–28.
[57] V. Kluck, C.K. Boahen, B. Kischkel, J.C. Dos Santos, V. Matzaraki, C.G. Boer, J.B. J. van Meurs, c. Genetics of Osteoarthritis, K. Schraa, H. Lemmers, H. Dijkstra, M. P. Leask, T.R. Merriman, T.O. Crisan, G.M. McCarthy, V. Kumar, L.A.B. Joosten, A functional genomics approach reveals suggestive quantitative trait loci associated with combined TLR4 and BCP crystal-induced inflammation and osteoarthritis, Osteoarthritis Cartilage 31 (8) (2023) 1022–1034.
[58] J. Yan, M. Shen, B. Sui, W. Lu, X. Han, Q. Wan, Y. Liu, J. Kang, W. Qin, Z. Zhang, D. Chen, Y. Cao, S. Ying, F.R. Tay, L.N. Niu, K. Jiao, Autophagic LC3(+) calcified extracellular vesicles initiate cartilage calcification in osteoarthritis, Sci. Adv. 8 (19) (2022), eabn1556.
[59] S. Gordon, Phagocytosis: an immunobiologic process, Immunity 44 (3) (2016) 463–475.
[60] R.S. Flannagan, V. Jaumouillé, S. Grinstein, The cell biology of phagocytosis, Annu. Rev. Pathol. 7 (2012) 61–98.
[61] A.G. Schwaid, K.B. Spencer, Strategies for targeting the NLRP3 inflammasome in the clinical and preclinical space, J. Med. Chem. 64 (1) (2021) 101–122.
[62] A. Serrano-Puebla, P. Boya, Lysosomal membrane permeabilization as a cell death mechanism in cancer cells, Biochem. Soc. Trans. 46 (2) (2018) 207–215.
[63] L.Y. El-Sharkawy, D. Brough, S. Freeman, Inhibiting the NLRP3 inflammasome, Molecules 25 (23) (2020).
[64] B. You, C. Zhou, Y. Yang, MSC-EVs alleviate osteoarthritis by regulating microenvironmental cells in the articular cavity and maintaining cartilage matrix homeostasis, Ageing Res. Rev. 85 (2023), 101864.
[65] J. Wan, Z. He, R. Peng, X. Wu, Z. Zhu, J. Cui, X. Hao, A. Chen, J. Zhang, P. Cheng, Injectable photocrosslinking spherical hydrogel-encapsulated targeting peptide-modified engineered exosomes for osteoarthritis therapy, J. Nanobiotechnol. 21 (1) (2023) 284.
[66] X. Xu, L. Xu, J. Xia, C. Wen, Y. Liang, Y. Zhang, Harnessing knee joint resident mesenchymal stem cells in cartilage tissue engineering, Acta Biomater. 168 (2023) 372–387.
[67] X. Xu, L. Xu, C. Wen, J. Xia, Y. Zhang, Y. Liang, Programming assembly of biomimetic exosomes: an emerging theranostic nanomedicine platform, Mater. Today Bio. 22 (2023), 100760.
[68] L. Xu, X. Xu, Y. Liang, C. Wen, K. Ouyang, J. Huang, Y. Xiao, X. Deng, J. Xia, L. Duan, Osteoclast-targeted delivery of anti-miRNA oligonucleotides by red blood cell extracellular vesicles, J. Contr. Release 358 (2023) 259–272.
[69] Z. Othman, B. Cillero Pastor, S. van Rijt, P. Habibovic, Understanding interactions between biomaterials and biological systems using proteomics, Biomaterials 167 (2018) 191–204.
[70] K. Jiao, M. Zhang, L. Niu, S. Yu, G. Zhen, L. Xian, B. Yu, K. Yang, P. Liu, X. Cao, M. Wang, Overexpressed TGF-β in subchondral bone leads to mandibular condyle degradation, J. Dent. Res. 93 (2) (2014) 140–147.
[71] N. Chen, Z. Ou, W. Zhang, X. Zhu, P. Li, J. Gong, Cathepsin B regulates non-canonical NLRP3 inflammasome pathway by modulating activation of caspase-11 in Kupffer cells, Cell Prolif. 51 (6) (2018), e12487.